上海交通大學

SHANGHAI JIAO TONG UNIVERSITY

学士学位论文

BACHELOR'S THESIS

论文题目：Development and Characterization of the Asymmetric Gas Jets for Electron Acceleration

学生姓名：刘泽洲

学生学号：5117319015

专　　业：物理学（国际班）

指导教师：Nasr A M.Hafz

学院(系)：物理与天文系

非对称喷嘴气体靶系统的开发与诊断

摘要

从工业界到科研界，气体喷射系统作为一个重要的仪器，被应用于很多工序或者实验中。在激光等离子体尾场加速实验中，气体喷射系统是组成气体靶的重要仪器。正因为气体喷射系统的重要性，如何诊断该系统，获得实验或生产所需的气体参数，成为气体系统相关行业不可避免的问题。本文就如何诊断气体系统给出了一套详尽的超声喷嘴实验，该实验系统基于干涉仪，所以不仅可以对气体，还可以对高速流动液体密度进行诊断。该实验包含了实验的构建到数据分析，可以作为一套标准化流程在各行各业中使用。因气体靶在电子尾场加速中有着十分重要的地位，本文也对电子加速的基本原理进行了简单的介绍。在该实验中，该文得到了氮气靶密度，气体压强以及空间分布之间的关系。同时，我们测得超声喷嘴产生的氮气靶密度的数量级为 10^{18} 到 10^{19} cm^{-3}。同时，对本诊断系统的改进构想在文章的讨论部分呈现。

关键词：气体喷射系统，干涉仪，激光等离子电子尾场加速，计算重构，超声喷嘴

Development and Characterization of the Asymmetric Gas Jets for Electron Acceleration

Abstract

Gas jet techniques are applied in many different areas ranging from industry to scientific research. Further, gas target is an essential component of the laser-driven electron acceleration. For the importance of the gas jet, the way to characterize a specific gas jet can be a ubiquitous problem in any relevant projects. This bachelor thesis gives an example for characterization of gas jet from experiment to data analysis, which can be referred to as a standard progress. In addition, simple idea about the laser plasma electron acceleration is also listed in this thesis, which is the main topic of gas target made for. For the experiment, the supersonic gas nozzle is characterized. We reconstruct the density profile of the gas target at different height for several gas pressures. Several clear correlations between the pressure, height position and density can be detected. More, the density of the Nitrogen gas target is in an order of 10^{18} to 10^{19} cm^{-3}. The further development idea can be checked at the end of thesis. This thesis provides an idea that the nozzles for varies demands can be easily analyzed.

Key words: Gas jet characterization, Interferometry, Electron acceleration, Computed Tomography, Supersonic nozzle,

Content

1 Introduction

1.1 Significance of this Research

The electron acceleration is one of the most important fields of physics in today's advanced world. High energy electron beam can generate a wide band-width radiation, which is from x-ray to THz wave[1]. Wide band width X-ray is the most applicable radiation in various researches and industries. Those applications make the electron accelerators0 important. For the space and mechanism reasons, the electron acceleration which is generated in the traditional RF accelerator is limited. Having started from last century, Dr. Tajima and Dawson proposed a new way known as the laser wakefield acceleration(LWFA) for electron acceleration[2], which uses the intense laser to excite plasma wave to accelerate electron, can obviously increase the electron acceleration gradient. From that time, many researchers devote in designing a compatible and powerful laser-driven accelerator[3].

The basic setup for laser-driven accelerator is composed of three main components, the laser system, target system and the diagnostic system. The laser used in LWFA is usually ultra-high intensity femto-second laser, which is developed in recent years[4]. The target systems are mainly classified into solid target and gas target based on which kind of material it uses for. In the ultra-short and ultra-high laser plasma electron acceleration experiment, the density of the plasma is one of the most important parameters which can impact on the electrons' kinetic energy. Since the density of the target has a relationship with the density of the plasma excited by the laser pulse[5], the method to characterize the gas target can significantly affect the accuracy of the result, that's the main

topic of this thesis. The diagnostic system usually is composed of energy spectrometer, beam profile monitor and laser diagnostic system. The whole system can help the acquisition of the experimental data and monitoring the whole system to ensure the proper function of all the other instruments. Gas target system is what this thesis works on.

Not only in research, in other aspects, gas jets are applied in many areas ranging from industry to research and span different sizes. Underdensed plasma target, which can be produced by the gas jet, have been used for compression of the laser pulse, changing of the laser frequency and enhancement of the laser intensity. All these applications make the gas jet important in different researches.

This bachelor thesis shows a way to build a characterization experiment setup and the algorithms which are needed to analyze the data. Moreover, this thesis can provide a standard procedure to get the density distribution and the profile of the gas target with a reasonable resolution and accuracy. Further, this setup not only can analyze the gas but also plasma since the diffraction differences between matter and vacuum not only appears in gas but other matters.

Honestly, there are some existing researches in the tomography of the gas target. For the cylindrical symmetric profile, the Abel Inversion method is preferred, which can reconstruct a symmetric density distribution[6-11]. However, in reality, since the edge of the nozzle can't be perfectly smooth, the profile of the gas target can varies a lot even there is a little spike at the edge. The high pressure of the gas and the structure of the supersonic nozzle make the gas target quite sensitive to the smoothness of the nozzle. From this point of view, precise reconstruction of the absolute density is a critical problem of the tomography. For the *asymmetric* gas target, more complex tomographic methods should be used. There are many different methods such as algebraic reconstruction techniques(ART)[12]. To overcome the uncertainty of the boundary condition of the gas target, *simultaneous iterative reconstruction technique*(SIRT) is widely applied.

In this thesis, I use the SIRT method to reconstruct the density distribution of asymmetric gas jet which is running in a vacuum chamber. The target I use is the rectangular slit nozzle. Also, to minimizing the error of the reconstruction, I also point out the method which should be used further.

1.2 Electron Acceleration

1.2.1 Background of the Electron Acceleration

Accelerator is one of the most important tools in both science researches and industries. In the public eyes, the Large Hadron Collider(LHC) at CERN maybe the most sophisticate one all over the world[13]. However, the smaller accelerator can always be the heart of many practical applications, like medical treatment or tele-communication. These days, researchers usually use the electron beam with high energy to produce radiation ranging from Soft X-ray to Terahertz wave to do their experiments which lie in widespread areas. It can be extremely useful if one can find a way to generate high energy electron beam in a limited space.

The topic of electron acceleration was founded in last century. At the beginning, researchers prefer the traditional Radio Frequency(RF)-based particle accelerator. There are three main parts of the RF-based accelerator, the linear accelerator, booster and the storage ring. The experimental stations are localized around the storage ring. However, this conventional technique is limited by both the size of the setup, the money for running this accelerator and the material to overcome the electrical breakdown.

A new technique was proposed to overcome the drawbacks of the RF accelerator. The pondermotive force of an ultra-high and ultra-short laser pulse can excite plasma wave, which can generate a high intensity electric fields, to accelerate the electrons. When a terawatt laser pulse is focused in a gas target, the prepulse of the laser can turn the target material to plasma. Then, the latter main pulse can

excite electrostatic plasma wave inside the plasma to localize and accelerate the electrons to relativistic energies in a relatively very small distance. This is a pretty famous tech named laser wakefield acceleration(LWFA) which was supposed last century. However, the mechanism for the acceleration is not that "fully understand" right now. We can already explain different phenomena with different theories though there are still some conflictions at the overlapping part of various theories.

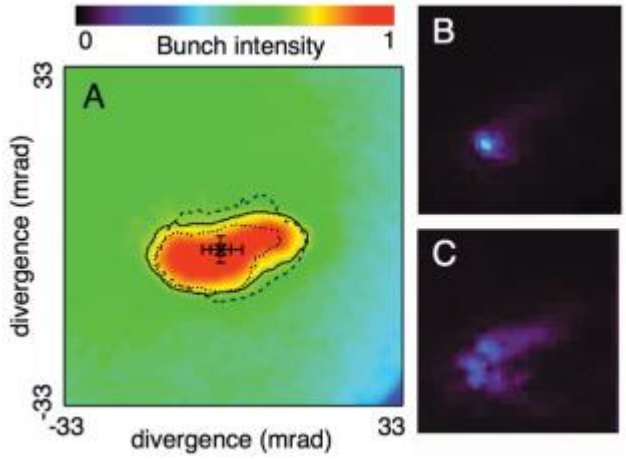

Fig[1.1].Electron bunch and transmitted laser profiles

Since LWFA has the potential in developing the next generation of the electron accelerator, the researchers working on this topic need to propose a way to make the acceleration tunnel longer and the acceleration gradient higher. To achieve their goal, an optimized laser system and a reasonable target system are always needed.

1.2.2 Simple Illustration of Laser-Plasma Electron Acceleration

To illustrate the principle of plasma electron accelerator, we must notice the plasma. "A plasma is a quasineutral gas of charged and neutral particles which exhibits collective behavior."[14]. Since the plasma consists of high concentration of charged particles, as these charged particles, like electrons, moves around the ions, they will generate a local concentration of chargers, which will generate an

electrical field. In this sense, we can go on the principle discussion.

If an ultra-high intensity laser pulse hit a plasma, due to the small mass of the electron, the electrons will be pushed by the pondermotive force which is generated by the gradient of the intensity of the laser. However, the mass of ions are much higher than that of the electrons. We can treat the ions as static. The electrons which are pushed out will be drugged back by the Coulomb Force from the ions. The momentum of the electrons causes them to overshoot and then oscillate around the ions with a characteristic frequency known as Plasma Frequency. The oscillation of the electron density, which is excited by the laser, can be treated as plasma wave.

If there is no consistently driving force, like continuous laser pulse, the plasma frequency can be calculated in the following formula[14]:

$$\omega_0 = (\frac{n_0 e^2}{\epsilon_0 m})^{1/2}\ rad/\sec \qquad (1-1)$$

Where n_0 is the equilibrium density of electrons, m is the mass of the electrons.

How to make the oscillation as big as possible? Obviously, we need the driving force has the same frequency as the plasma frequency, that is, the laser pulse duration should satisfy:

$$\omega_0 * \tau = 1 \qquad (1-2)$$

Where τ is the duration of the laser pulse.

With the proper laser system, the powerful electric fields can be set in the plasma wave. Theoretically, we are more interested in the time-average electrical field in the plasma wave. Since the pondermotive force is the one causes the shifting of the electrons, the following relationship should be satisfied:

$$E_{ave} \propto F_{pon} \propto -\nabla I \qquad (1-3)$$

Where I is the intensity of the laser pulse. The derivation is as follow:

For the single electron, from Newton's Law, we know that:

$$\frac{d^2\vec{r}}{dt^2} = \frac{q}{m}\left(\vec{E}\left(\vec{r}\right) + \frac{1}{c}\frac{d\vec{r}}{dt} \times \vec{B}\left(\vec{r}\right)\right)e^{-i\omega t} \qquad (1-4)$$

Since the motive is the combination of the oscillation $\vec{r_0}$ and motion of the ion $\vec{r_1}$. We assume that:

$$\vec{r} = \vec{r_0} + \vec{r_1} \quad (1-5)$$

We can treat the oscillation as the perturbation of the ion motion. Expand the $\vec{E}(\vec{r})$ with Taylor Formula, we have:

$$\vec{E}(\vec{r}) = \vec{E}(\vec{r_1}) + (\vec{r_0} * \nabla)\vec{E}(\vec{r_1}) \quad (1-6)$$

And the oscillation is with the plasma frequency. We have:

$$\vec{r_0} = -\frac{q}{m\omega^2}\vec{E}(\vec{r})e^{-i\omega t} \quad (1-7)$$

Which is simply the result by taking the integration for the Newton's Law. By substituting the relationships above to the motion equation, we have:

$$\ddot{\vec{r}} = -\frac{q^2}{4m^2\omega^2}\nabla E^2(r) \quad (1-8)$$

Thus we have the linear relationship sequence above.

The electrons with high kinetic energy should be injected to the plasma wave in the right phase. However, due to the acceleration always need high intensity laser, there already have been some highly energetic electrons in the background. This reduces a difficult procedure researcher should do.

The electrons in the background can be accelerated by the plasma wave, which is generated by the main pulse. For different research proposes, the target varies a lot. Some groups use the air as the gas target, others maybe more interested in the vacuum chamber. The energy spectrum of the electron beam varies a lot with the different material of the target. This is also an interesting topic in this field.

1.2.3 Challenge in the application of the Laser-Plasma Electron Accelerator

There are many potential applications of laser-plasma electron acceleration, like the radiography for medical diagnosis, radiotherapy, material diagnosis and basic study in the nature of plasma. However, there are still many challenges in this field, mostly about the laser system. Reducing the energy fluctuation from shot to shot, increasing the intensity of the laser beam, minimizing the size of the laser

system are the important but not all the problems we need to fix before this technique can be applied.

Laser-plasma electron acceleration is relatively a new technique since it only appeared like 40 years ago. It has the undeniable advantage than the traditional synchrotron radiation source. Further development of this tech can be expected.

1.3 Target System

1.3.1 Solid Target System

Solid target system is the traditional target for the electron acceleration. As soon as the ultra-high intensity laser hit the surface of the target, the pre-pulse can generate a plasma layer at the surface of the target. The atoms at the surface of the target will be ionized to ions and electrons. The density of the electron satisfies the definition of the plasma. That plasma is qualified enough for the electron plasma wave generation. Then the main pulse of the laser can excite an oscillation of the electron density distribution, which is the source of the electron acceleration.

However, for a solid target, the plasma density is the key for the acceleration. Once the density is higher than the critical density, the laser beam will be reflected like a beam hit a mirror. For the solid target, we have[15]

$$\omega^2 = \frac{4\pi e^2 n_c}{m} \qquad (1-9)$$

Where ω is the frequency of the laser and n_c is the critical density of the plasma. Reversely, we can calculate the critical laser for a specific laser wavelength is: [Paul.Gibbon Short Pulse Laser Interactions with Matter, page128]

$$n_c \approx 1.1 * 10^{21} (\frac{\lambda}{\mu m}) cm^{-3} \qquad (1-10)$$

We can get the estimation result that the density of the plasma created by the solid target is higher than the critical density. This means the electromagnetic wave is

shot to a highly overdensed plasma, just like a mirror. In this sense, solid target is not a good target for the electron acceleration. The acceleration channel which is produced by the LWFA mechanism can only appear at the coronal layer of the plasma from solid.

1.3.2 Gas Target System

Compared to the solid target system, the gas target has the advantage that the repetition rate is higher, the density of the gas is relatively stable and the plasma density is underdensed. Also, it's much easier to change the gas than to order a customized solid target.

Theoretically, the most important advantage of the gas target is that it can extend the length of the plasma channel, which can significantly optimize the energy of the electrons[16]. For this reason, gas target experiment is extremely popular in this field. Moreover, the interesting thing is, we can use different methods to manipulate the density distribution of the gas target, so that we can find the most adequate gas target profile for the electron acceleration. For example[17][18] , the research group at Lawrence Berkeley National Laboratory did an experiment that they use a double slit nozzle to create a density ramp at the valley of the two opening. The result shows that the electron with about 1MeV mean energy and the 10 times lower momentum spreads both with longitudinal and transverse direction. Latter, the group in UK STFC Rutherford Appleton Laboratory gives out the particle-in-cell(PIC) simulation to illustrate the experiment. The result also showed that the separate injection stage works much better than the single slit. The momentum spread with peak-valley-peak target is much smaller than the Gaussian form target. For this, we can see that the gas target has the potential to be manipulated in both profile and density, which is obviously important for the electron acceleration.

In our case, we use the Nitrogen gas as the target material. To reduce the

difficulty of the experiment, we choose the single slit stage for test. Our nozzle is a supersonic nozzle, which means the gas should be applied with the compressible gas theory, not the conventional fluid dynamics. The supersonic nozzle has a throat in the middle of the gas channel. The pressure gradient from the throat to the opening is relatively huge compared to the usual gas nozzle. However, the velocity of the fluidic elements is beyond that of the sound. The details are explained at the experimental setup part. From the equation we have, we can see the density of the plasma is lower than the critical density when the femto-second laser is applied, which means the target is suitable for the experiment.

1.4 Characterization of the Gas jet

1.4.1 Different Experiment setups

The experiment setups for the characterization of the gas jet vary lot. However, the basic principles are roughly the same. Interferometric method is the standard way to measure the density of gas or liquid. Here, the principle of the interferometry and several different setups for the interferometry will be shown as follow.

Interferometry is a technique to extract the phase information of the interference pattern. In Young's interference experiment, the bright and dark inference fringes are formed based on the phase difference of two identical beams. In 1883, Albert Abrahan Michelson proposed an interferometer to measure the refraction rate, wave length and many other characteristic properties of the light based on the Young's interference experiment. The Michelson interferometer uses the principle of the superposition. It can split a single incoming coherent beam into two different paths. After traveling different beam path, two beams will be

recombined into one beam at the detector. Since these two beams pass through different paths, they will have different phases, which can affect the interference pattern at the detector.

Suppose we put a transparent object (glass for example) which has a higher refraction index than the vacuum into one of the beam path, if the size of the beam is reasonable large enough to cover this entire object, we can clearly see the shift of the fringes since the phase of the beam changes due to the object. After some procedures, we can read out the phase information from the interference pattern. In other words, we can "extract" information we want from the fringe shift. This is very critical for the interferometry.

The interferometer should have at least two abilities. The first one is the ability to generate two coherent signal beams. The second one is the ability to produce a phase shift from the probing object. Actually, there are many kinds of interferometers which can satisfy these two requirements, like Fizeau interferometer, Mach Zehnder interferometer and Fresnel Biprism interferometer.

1.4.1.1 Fizeau interferometer

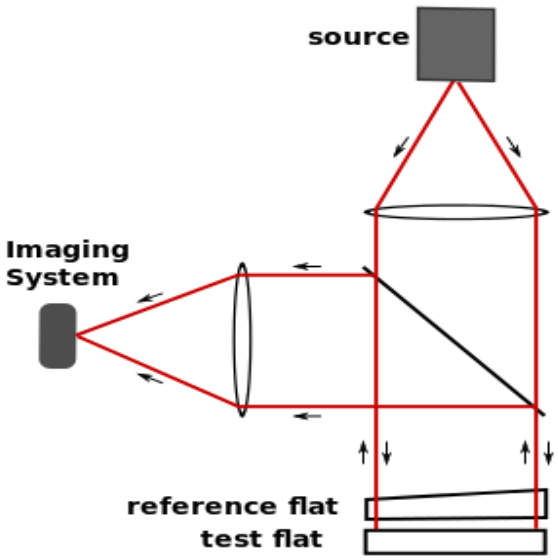

Fig[1.2].Illustration for Fizeau interferometer[19]

The beam splitter inside the interferometer splits the beam into two branches.

These two beams can interfere at the imaging system. The lens before the imaging system is the eyepiece of the imaging system. The lens after the beam source is used as a beam collimator.

1.4.1.2 Mach Zehnder interferometer

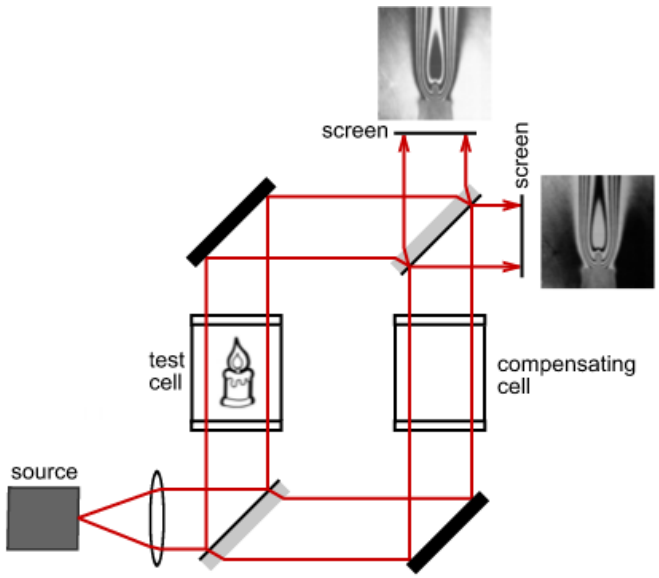

Fig[1.3]. Illustration for Mach Zehnder Interferometer[20]

Mach Zehnder interferometer also uses a beam splitter to generate two coherent beams. The different of the refraction index between the test cell and compensating cell can tilt the fringes at the screen. This setup provides large space for test object and two different output patterns. The imaging system is omitted as screen.

1.4.1.3 Fresnel Biprism interferometer

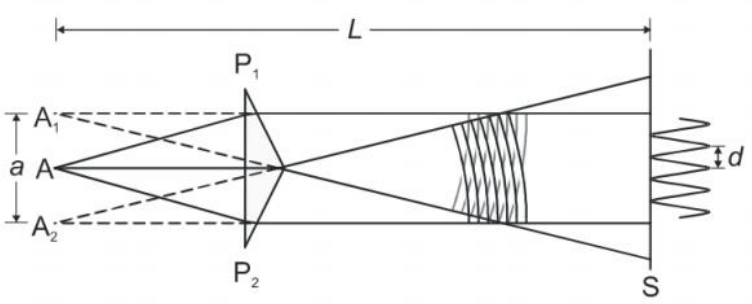

Fig[1.4].Illustration for Fresnel Biprism Interferometer

Fresnel Biprism uses a biprism to generate two coherent light sources from one. The mechanism of this interferometer is much like what was proved in Young's interference experiment. We can put our test object into the main beam to see the fringe shift. This setup has the advantage that it can provide the highly coherent sources and it can operate in a limited space, which is compatible with the size of our gas jet. In our case, we chose to use the Fresnel biprism system to get the interference pattern.

1.4.2 Different Analyzation Algorithms

The algorithm for the reconstruction of the gas jet density is mainly composed of two parts, which are the phase calculation part and the tomography part.

What we can get from the experiment is the interference pattern with some shifted fringes. From these graph, we need to carefully follow a sophisticate procedure to get the accurate density result.

The first procedure is to read out the phase shift from the interference pattern. From the basic optics book, we know that the brightness of the pattern represent the active phase. The phase is periodically changing from $-\pi$ to π [21]. This progress can be divided into image enhancement part and phase unwrap part. The Fast Fourier Transform(fft) will be performed on the 2D data. The zero frequency and high-frequency which means the noise will be filtered out. Then the Inverse fft will help to get the filtered patterns. Since the wrapping phase can only range in $[-\pi,\pi)$, we need to get the absolute phase of the map. The unwrapping algorithm is involved here. The algorithm I chose is the *Goldstein 2D Unwrapping Method*. This method can significantly reduce the noise that appears in the phase graph. The details will be listed in the data analysis part.

After those steps, the tomography parts are in consideration. In general, many interference patterns from different angles are needed to reconstruct the density profile accurately. For instance, Computed Tomography(CT) techniques in medical treatment detect patients' bodies in different perspectives with x-ray to help doctor make a diagnosis. The same situation lies here. However, since the shape of a gas nozzle has a rectangular shape, two angles patterns are sufficient enough to get a reasonable result.

However, the tomography method varies from analytical reconstruction to algebraic reconstruction. The analytical one needs the complete boundary conditions, which are usually not available in real experiment for the data acquisition problem, but it has the fastest calculation speed. Moreover, the algebraic reconstruction need less boundary conditions. It needs iteration times to make the reconstruction result compatible with the images obtained from the experiment. The main idea of the algebraic reconstruction is taking average of the facts we have. Once we find the reconstruction is compatible with the fact, the tomography is achieved. This ubiquitous formula is:

$$x^{k+1} = x^k + \lambda_k \frac{b_i - \langle a_i, x^k \rangle}{\|a_i\|^2} a_i \qquad (1-11)$$

Where x is the reconstruction result, k is the iteration time, λ is the relaxation parameter ranging in (0,2), i is the index for the image we have, a_i is the area of the reconstruction matrix, the $\langle a_i, x^k \rangle$ is the result for the pattern with the reconstruction result in k times. This formula gives an iteration routine for tomography. The more advanced methods are always based on this idea and plug some prior knowledge into the algorithm.

The tomography algorithm shown in this thesis is named Simultaneous iterative reconstruction technique(SIRT). I performed *SIRT with Optimized Goldstein 2D Unwrapping* to characterize the rectangular gas jet we have. All the other parameters and details about the algorithm and experiment setup can be found in experiment and data analysis part.

2 Experiment setups

2.1 Laser system

The laser system we used in experiment as a monochromatic coherent light source is an unpolarized He-Ne laser with 632.8nm wavelength which is supplied by Thorlabs. The laser can be shown as follow:

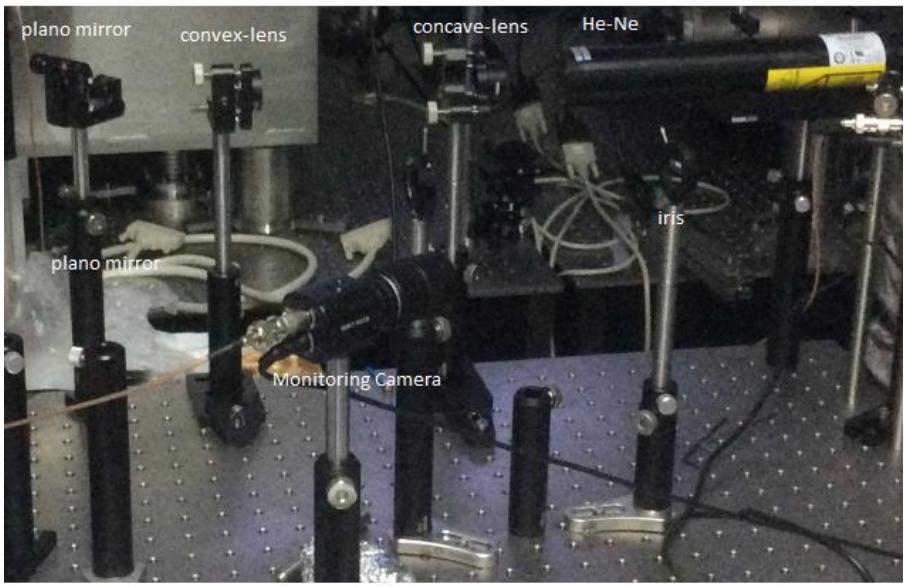

Fig[2.1].Laser System

The common specifications of the laser is listed here. The mode structure is TEM00>95%. The divergence of the beam is less than 1.7mrad, however, we can adjust the divergence by the collimator. The frequency is in the order of 100MHz, which means we can treat the laser as continuous light source.

The He-Ne laser is set at the right upper corner of the figure shown above. Since the laser itself has little divergence, we put a pair of lens after the laser to help control the beam size and the collimation. The plano mirrors pair is for changing the beam line. In order to have a high quality beam spot, we use an iris to cut the center part of the spot. The beam size here is ensured large enough to cover the size of the gas nozzle, so that we can get a convincible result which contains all

the information we need for reconstruction. Monitor Camera is for checking whether the beam line is tilting or not.

After all the pre-treated of the laser beam, we can get a horizontal and collimated beam which is ready for the detection of the gas jet.

2.2 Fresnel Biprism Interferometer

Fresnel biprism interferometer is an experiment setup based on the Young's Double Slit Experiment. As the principle shown before, we used a convex lens to focus the beam before the biprism. Then we can adjust the distance between the biprism and the lens to adjust the distance between the interference fringes. From the double slit experiment, we know:

$$\Delta x = \frac{\lambda D}{d} \qquad (2-1)$$

Where Δx is the distance between two adjacent fringes, D is the distance between the detector and the double slit and, d is the distance between two slits. In our experiment, we set the CCD camera and laser fixed, so that d is the only parameter which can affect Δx.

We can know that d will get smaller with the distance between the focus and biprism get larger. Based on this qualitative relationship, we can adjust the biprism to get a reasonable resolution of the result. Of course the resolution of the CCD should also be considered. To help imaging the fringe patterns to the CCD, we also put a double lens system after the biprism. After adjusting the lens and the position of the biprism, we finally got the reasonable result.

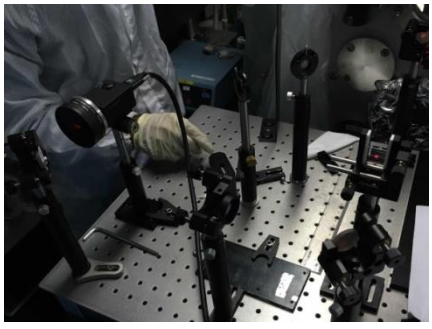

Fig[2.2].Imaging System

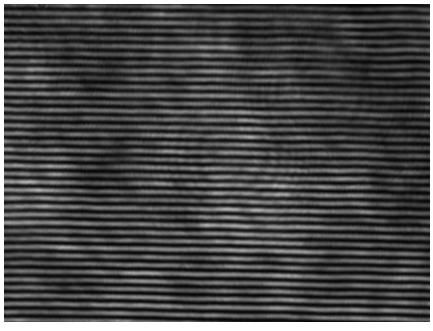

Fig[2.3].Sample Interference Pattern

2.3 High Pressure Gas Jet System

Due to the function of the gas jet, we can adjust the pressure of the gas coming out. The range for the gas is from 1 to 100 bar. The gas jet is shown below:

Fig[2.4].Nozzle profile

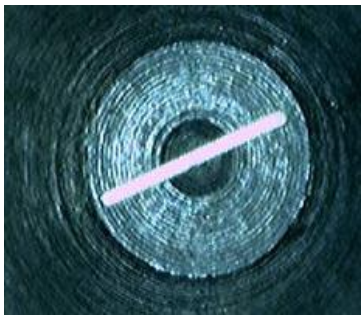

Fig[2.5].Orifice profile

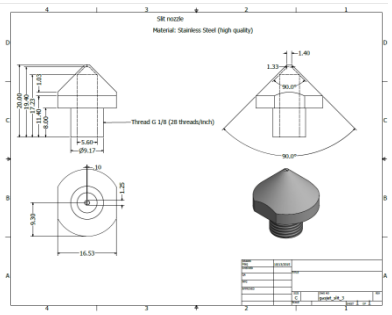

Fig[2.6].CAD graph

We designed the gas nozzle by ourselves with Solidworks, and ordered the parts from different manufacturing companies, so that we can get the ideal gas targets with different profiles. One of the key here is that the characterization of the *asymmetric nozzle* is needed. From the instruction of the gas jet system, we figure out that the area of the nozzle should be a constant. Otherwise the system can't stop the gas ejection. In the graph, we fixed the multiplying result of the width and length of the gas nozzle to make sure the system is working. On the other hand, the characterization of the asymmetric nozzle is relatively important since that's where this thesis mainly working on. We treat the nozzle very clearly to guarantee the success of the experiment.

We can also change the trigger time difference between the CCD camera and the gas jet. In this sense, we can investigate the time evolution of the density for the gas target. But in this experiment, we use the gas target for generating plasma, the time for laser is in femtosecond scale, however the accuracy of the gas jet trigger is in millisecond scale. We only have an optimization in experiment by our observation of the interference pattern. Further, we are able to choose a reasonable time for the main laser pulse when do the acceleration experiment, though it's not that accurate.

The nozzle we used is order from *Shanghai Ronggao Laser Manufactory Co.,ltd.* They use the high intensity continuous laser to remove the material from the base. In general, this method can work well in the precision about 1um. The material we use is high quality stainless steel which is popular around the lab. The CAD graph and the test images are shown above. Under the microscope measure, we find that the gas nozzle has a good smoothness and low error compared to the graph. This part is qualified for the experiment.

2.4 Summary of the Experimental Setup

A summary of the total experimental setup should be presented here. The Beam path is shown below:

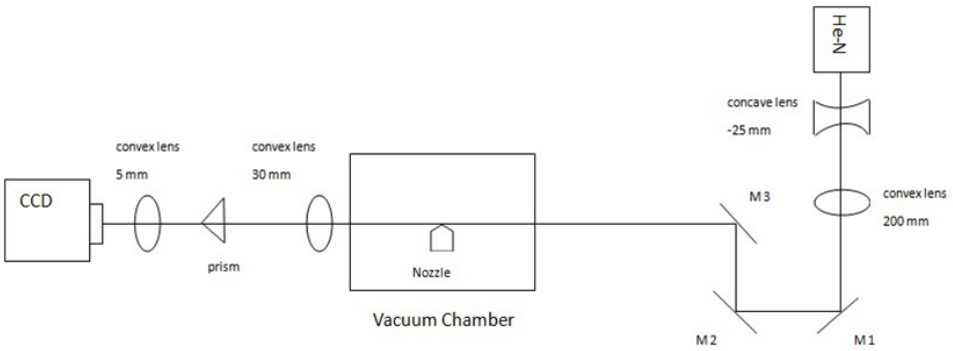

Fig[2.7].Illustration for the beam path in experiment

The laser is coming out from the He-Ne laser. Then the beam is adjusted by the collimator which is composed of a convex lens and a concave lens. Then the detection beam is changed the direction of the wave front by M1 M2 and M3. In summary, the laser system prepares the laser before the beam probing the vacuum chamber. Next the laser is passing though the target. Inside the chamber, there are two big planar mirrors which are larger than those of the laser system at the corner of chamber. Since the reasonable beam size should be compatible with the size of the nozzle, the beam spot is a little bit larger than the usual mirror. Also, the gas jet system is installed on the electrical target mount through a feedthrough on the wall of the chamber. After this, we know that the beam front is not planar

wave front. There must be phase shift compared with the background. Then the double lens imaging system is working. Since we have limited space in the optical table, the double lens imaging system can significantly reduce the imaging distance. This can make sure we can get a clear real image in CCD's chip. This step is fairly important, because it can influence the accuracy of the result directly.

Moreover, to ensure the beam's wave front is not changed and use the limited space efficiently, we added two planar mirrors and a double lens imaging system before the CCD, which shows a great success in experiment. The double lens system can reduce the distance needed for the experiment. The magnification and resolution can also be taken into consideration. From the simple optics, we know that:

$$\frac{1}{u}+\frac{1}{v}=\frac{1}{f} \qquad (2-2)$$

Where u is the object distance and u is the image distance. f is the focal length. We can set the image generated by the first lens as the object for the second lens. Thus, the calculation is relatively simple. The calculation is done by my colleague Xia. He made a convenient program to calculate the distance and the magnification for the lens pair. This program makes the experiment relatively easy for adjusting the lens and the distance.

During the experiment, we take the background and get the data for different pressure and delay time. After finding the most suitable delay time, which is 15ms, we fixed the CCD trigger time and assume this is the optimized time for the electron acceleration experiment. Then we trigger the system from the gas jet system. The gas jet system itself can generate a trigger signal for the subsequent experimental instruments. All of the data is get with the same setup.

3 Data Analysis

3.1 Outline of the Procedure

The procedure of the data analysis is divided into two main parts which are the image processing part and the tomography part.

Image processing part is mainly concerned about the image enhancement, FFT, filtering, iFFT and unwrapping. From image enhancement to iFFT, the procedure is to reduce the noise which is generated from the experiment. Unwrapping is to get the absolute phase information from the data. The important thing is the data we got should have a high quality. High quality here means that the data satisfies the Nyquist Sampling Theory, which is ubiquitous in any signal processing job.

After processing the row data, we can get the absolute phase difference distribution in different heights and perspectives, which in our case are the front view and the side view. Since we know there is a relationship between the phase difference and the refraction index, we can calculate the index of the gas target. Then, referring to the gas and laser property, we can easily calculate the density. That's the basic idea for the method. Although there are many detailed problems to be fixed in order to have a good result, the principle of the idea is pretty straight forward. However, in reality, we prefer SIRT method since it has a good convergence stability. SIRT only needs around 200 iteration times to get a result with error less than 1%.

By applying SIRT, we can get the density distribution in a specific height from processing the front and side view data. Then we will investigate the property and profile of the gas target. Find the possibility to build a ramp between two slit. The job is done here.

The sample image we get from the experiment is shown below:

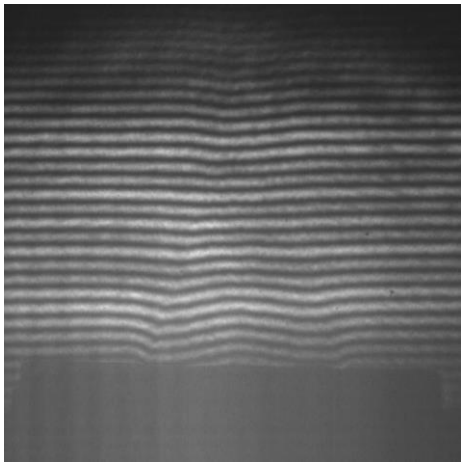

Fig[3.1].Interference pattern(front)

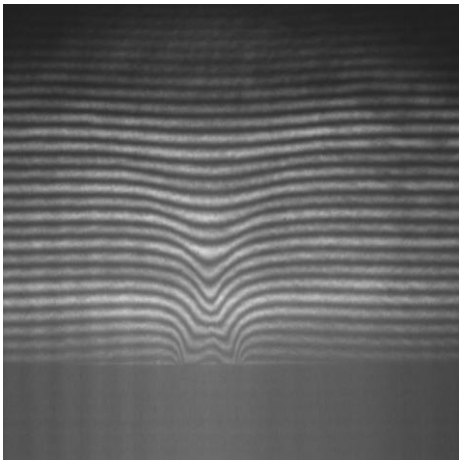

Fig[3.2].Interference pattern(side)

3.2 Image Enhancement and Filtering

Image enhancement and filter is a pretty standard procedure. As we know, in experiment, the noise always shows at every acquisition instrument, especially for the image acquisition. In the data analysis, the best we can do is to reduce the noise by the scientific method. Fourier analysis is an outstanding tool to filter the noise out. In reality, the noise is usually with a high frequency but low amplitude form in the frequency domain. Fourier analysis is needed in this method. For the image, the 2D Fourier Transform is applied. In my understanding, 2D FFT is nothing but do the usual Fourier analysis in both axis of the image. For 2D FFT, we know that the intensity can be expanded as:

$$i(x,y) = i_0(x,y) + \int m(v_x, v_y) * \exp(i2\pi v_x x + i2\pi v_y y)\, dv_x dv_y \quad (3-1)$$

Where $m(v_x, v_y)$ is complex coefficient of frequency v_x and v_y. In our row data, when there is no gas ejected out, the fringe pattern should be uniformly distributed with the same frequency. There shouldn't be any deviation spots near the 1st frequency line. And when there are gases coming out, there will be some shifts around that basic frequency. In other words, there should be a cluster of spots around the first frequency.

The zero frequency, which is named as "DC current" in Fourier analysis, contains

no information at all. As we know from the basic fourier analysis, the "DC current" should be filtered out. In this sense, we use a small box mask to take the first frequency out only. The other terms are not included here. Moreover, the size of the rectangular box is related to the resolution of the data output, which is shown below. Right now, we are at the position to derive the function for the transformation. We can derive $m(v_x, v_y)$ from the equation above by multiply the base parts and take integral both sides:

$$m(v_x, v_y) = \iint \exp\left[-(i2\pi v_x x + i2\pi v_y y)\right] * i(x, y)dxdy \qquad (3-2)$$

This is the basic principle of the 2D Fourier Analysis. In general, we say that a function is transformed to a different one. The operation is reversible. In this sense, we need to transform the spatial data into frequency domain to do the filter. Then we do an inverse transformation to get the noise free data. In practical works, we perform fft2 function on the data we have to get the frequency spectrum. The algorithm inside the Matlab is sophisticate enough for this task. It chooses a reasonable step length for the gradient calculation and integral calculation, which make the process convincible. The result we got is as follow:

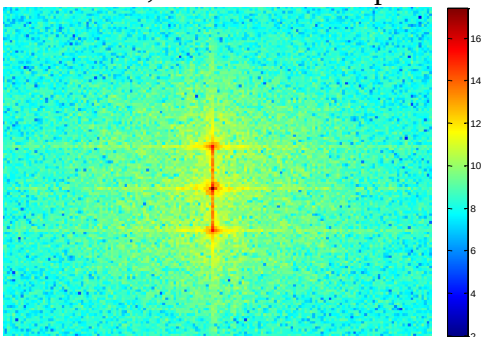

Fig[3.3].Background Frequency(front)

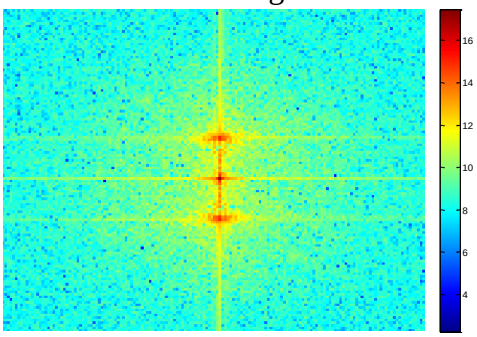

Fig[3.4].Shifted Frequency(side)

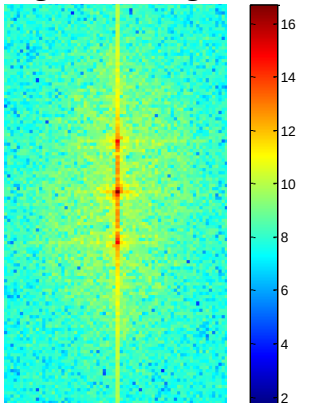

Fig[3.5].Background Frequency(side)

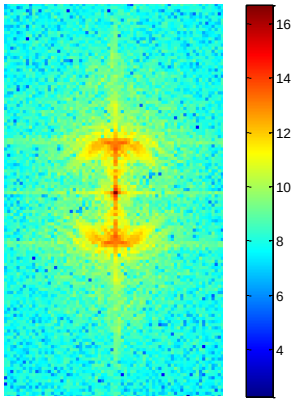

Fig[3.6].Shifted Frequency(side)

We can see clearly the difference between these two groups at the 1st frequency. The background frequency map has a more clear 1st frequency since all the fringes are evenly separated. The shifted frequency map has more perturbation around the 1st frequency. This is reasonable since the fringes are shifted by the refraction index of the gas, which changed the frequency somewhere in the row data. We can say that the information we need is contained in the area around the first frequency. So our method to reduce the noise is to use a mask to take the information part out. Here, as the thesis mentioned before, the larger box will lead a finer resolution. However, limiting the size of the mask can reduce the error created by the imperfection of the beam. Practically, we choose an intermediate size box mask to filter the frequency. Then, we use the inverse FFT to get the phase maps of both background and shifted pattern. Right now the phase map should be complex since we filter the noise out. To calculate the phase, the function below is applied:

$$\varphi = \arctan\left(\frac{Im(phase)}{Re(phase)}\right) \qquad (3-2)$$

However, the arctan we used should be the quartic form since the data is 2 dimensional. The phase information in the data is suitable to do the quartic arctan calculation. The quartic arctan function can not only calculate the arctan value, but only compare the result with the adjacent points. This method can expand the value region of the arctan and give out a more precise output. The quartic arctan function spans [$-\pi, \pi$). In Matlab, the function is arctan2, which is also suitable enough to do this job. Then we deduct the background phase map from the shifted phase map. We got:

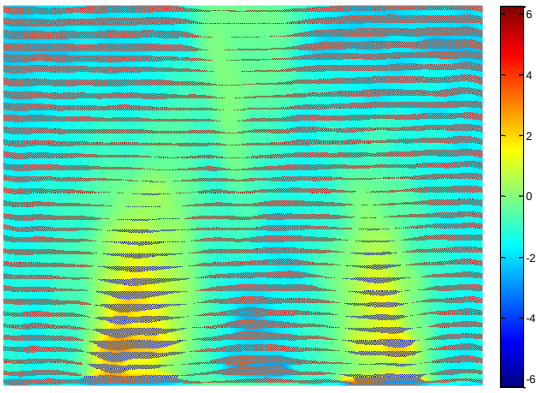

Fig[3.7].Wrapping phase map(front)

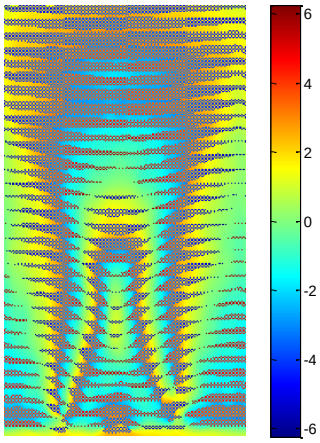

Fig[3.8].Wrapping phase map(side)

Since the quartic arctan function span only [$-\pi$, π), the phase map we got is wrapped. The wrapping phase we showed above is the pure phase difference. It means we subtract the background phase from the shifted phase. That's the reason why the range varies from [-2π, 2π) . Actually we can't read out the absolute phase difference from the graph. For example, if the real phase difference is 3π, in the case above, we can only got π, which is obviously wrong. To "unwrap" the phase, we carry out two methods. One is using 1D unwrapping function to every column. Actually, if the quality of the row data is good, which means there is no punks on the map, this method would be robust enough. However, in our calculation, the data is not perfect. It's very essential to use the Goldstein unwrapping algorithm to reduce the error.

3.3 Goldstein Branch-cuts based Phase Unwrapping

To carry out the tomography, what we need is the unwrapped phase map. However, what does the "unwrap" mean?

At the beginning of the part, I should introduce a simple theory named Nyquist Sampling Theory.

Nyquist-Shannon Sampling Theorem is a fundamental bridge between the analog signals and the digital signals. It shows a sufficient requirement for sample rate

that allows the digital signals capture all the information from the analog signal of finite bandwidth. The proof is easy to find in any text book. Here all we need to know is that the frequency of the phase detection is at least two times of that for the phase shift for the gas. Actually, in reality, we always choose at least 10 times acquisition frequency as the proper digital signal. The method to analyze the map's quality is shown as follow. This theorem is essential in our work.

As the thesis presented before, the quartic arctan function can only get a result in the range [$-\pi$, π). However, sometimes this range is not compatible with the real result. Range is not big enough to include all the phase data value. Consider the following sequence of phase:

$$-3, -1, 1, 3, -2, 0, 2, -1.5.0.5, 2.5 \ldots$$

We can see clearly that this sequence has a range not smaller than [-3,3]. However, we see by our feeling that the sequence is increasing except for two discontinuous points. We can see that the 5th point is at the next cycle of the 4th point, which means the latter one is wrapped with one cycle. To illustrate the idea more clearly, I prefer to draw the graph out:

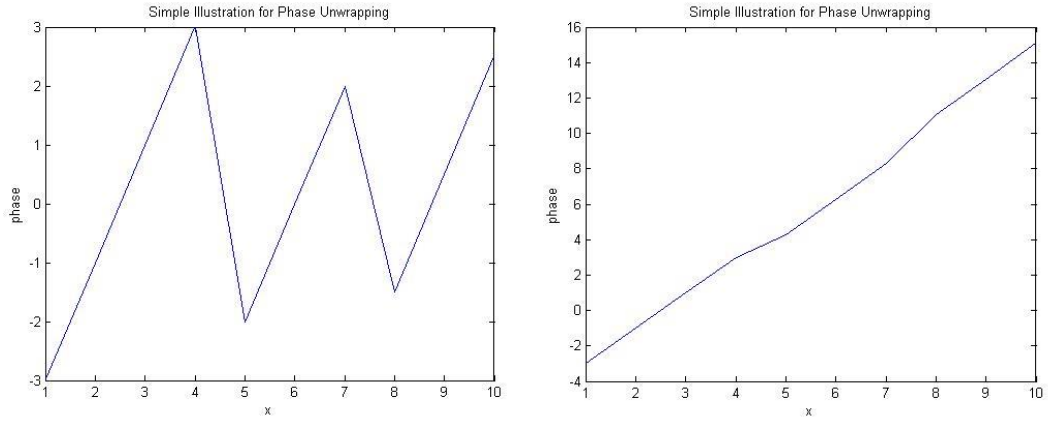

In the graph, the x axis is the index number of the virtual data. y axis is the virtual phase number. The line connecting points is just for illustration need.

In the first illustration graph, there is a discontinuity between both the 4th and 5th data points and 7th and 8th data points. In practical measurement, we always assume that our detector has a fine resolution which can continuously measure the phase. Continuous measurement here means the difference is less than half a

cycle, which is proved by Sample Theory in any signal processing textbook. So, in this situation, we can illustrate the reason why this phenomenon appears here. Assuming the data is qualified enough, the difference between two wrapped points should be larger than half a cycle.

We can observe the sequence above, apparently the 5th data points is missed 1 cycle. It's clearly that one cycle should be added to the 5th to 7th data and two cycles should be added to get the real phase information which is shown in the second graph.

To illustrate the branch cut unwrapping theory, suppose an operator ζ. When operator ζ works on the unwrapped phase map, it can generate the wrapped phase map, which in our case the row data.

$$\zeta(P)\ is\ the\ row\ data\ we\ get\ from\ experiment$$

The way to do this job is to add the integer cycles that minimizes the gap between two data points. In our condition, the function is as follow:

$$\Delta = P(i+1) - P(i) \qquad (3-3)$$

$$P(i+1) = \begin{cases} \zeta\left(P(i+1)\right) - 2\pi * floor((\Delta + \pi)/2\pi) & \Delta > 0 \\ \zeta\left(P(i+1)\right) - 2\pi * ceil((\Delta - \pi)/2\pi) & \Delta \leq 0 \end{cases} \qquad (3-4)$$

Where the phase(i) is already unwrapped. Of course, the profile of the function is the same with y=x.

Theoretically, if the unwrapped phase map has a high resolution and is a "real map", "real" here means it is taken from reality, which means the absolute phase is smooth, we can directly do the unwrapped for the leading columns(or rows) then unwrap all the rows(or columns) of the graph. The result should be the same. However, there are two possible errors which may appear in the data acquisition. The first one is the noise, which is named as "local error"[22]. The second is generated by the propagation of the local error. As we can see from the unwrapping function, the data points is processed one by one, which means the local error can propagate and accumulate as the data processing.

To minimize the effect of these errors, we use a method called “Branch Cut”. The branch cut line is areas in the data map which the unwrapping can’t propagate through. First, assume we have a fine resolution data. To define “fine resolution” mathematically, we assume the difference on the unwrapped phase between two adjacent pixels is less than half of the cycle, which means π in our case, which is also called Nyquist Sampling theory. In Nyquist Sampling Theory, to reconstruct the signal unambiguously, the acquisition frequency of the instrument is at least two times as the data frequency. In our case, the period of the fringe patterns is 2 π, so, at least, we need:

$$|P(\vec{r}+\hat{e})-P(\vec{r})| \leq \pi \qquad (3-5)$$

Where P is the unwrapped 2D phase data. The noise coming from the data acquisition appears when there is an actual discontinuity in phase, which means the difference is larger than π. When this happens, the signal is not qualified to reconstruct the original signal correctly. We can treat this data point is “bad” and mark it by “branch cut”.

Since the unwrapped phase is continuous, we have:

$$P(\overrightarrow{r_1}) = \int_{r_0}^{r_1} \nabla\vec{P}(\vec{r}) * dr + P(\overrightarrow{r_0}) \qquad (3-6)$$

$$\oint \nabla\vec{P}(\vec{r}) * d\vec{r} = 0 \qquad (3-7)$$

If the circular integral is not zeros, there must be a gap which doesn’t satisfy the Nyquist theory. The minimum integral path is the circle made by the four adjacent fours. So, the strategy is that, first, unwrap the four points based on the left upper corner point. Then, calculate the circular integral. There should be only 2π or -2π for the residue, otherwise the quality of the row data is far from Nyquist Theory. The equation I used is as follow:

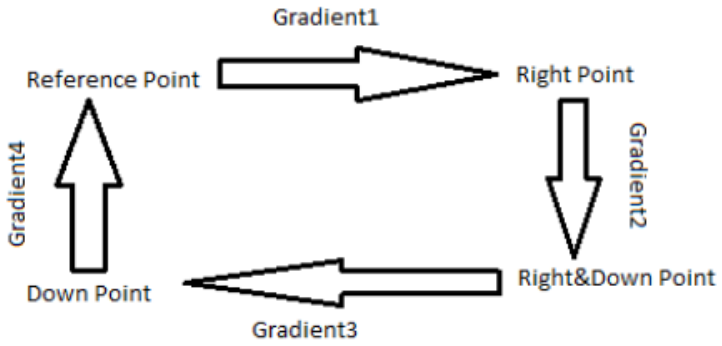

Fig[3.9]. Illustration for the charge calculation

$$Gradient1 = P(Right\ Point) - P(Reference\ Point)$$
$$Gradient2 = P(Right\&Down\ Point) - P(Right\ Point) \quad (3-7)$$
$$Gradient3 = P(Down\ Point) - P(Right\&Down\ Point)$$
$$Gradient4 = P(Reference\ Point) - P(Down\ Point)$$

To illustrate it more clearly, maybe I need to use a clearer example. Suppose the circular integral of four points is as follow:

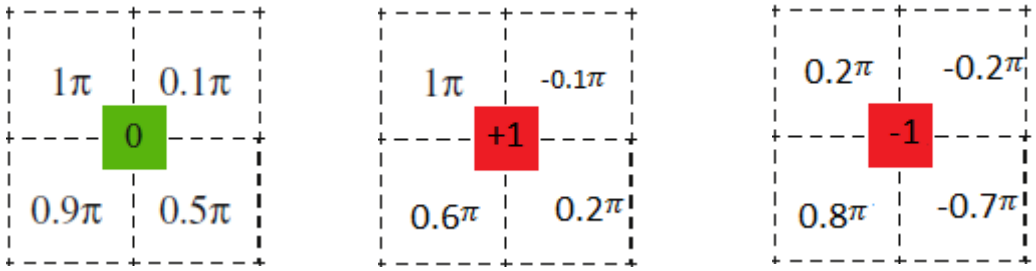

Fig[3.10].Illustration for the Branch Cut charge calculation

In the first figure, we can check that difference between two adjacent points is not bigger than π. So that we can calculate the different directly. The charge for this one is 0. For the second graph, we calculate the gradients seperately.

$$Gradient1 = -0.1\pi + 2\pi - \pi = 0.9\pi$$
$$Gradient2 = 0.2\pi + 0.1\pi = 0.3\pi \quad (3-8)$$
$$Gradient3 = 0.6\pi - 0.2\pi = 0.4\pi$$
$$Gradient4 = \pi - 0.6\pi = 0.4\pi$$

So, the circular integral is equal to:

$$\oint \nabla P(\vec{r})dr = 0.9\pi + 0.3\pi + 0.4\pi + 0.4\pi = 2\pi \quad (3-9)$$

Then we mark the charge of this cell as +1. Similarly, for the last one,

$$Gradient1 = -0.2\pi - 0.2\pi = -0.4\pi$$
$$Gradient2 = -0.7\pi + 0.2\pi = -0.5\pi \quad (3-10)$$
$$Gradient3 = 0.8\pi - 2\pi + 0.7\pi = -0.5\pi$$
$$Gradient4 = 0.2\pi - 0.8\pi = -0.6\pi$$

So the circular integral is:

$$\oint \nabla P(\vec{r})dr = -0.4\pi - 0.5\pi - 0.5\pi - 0.6\pi = -2\pi \quad (3-11)$$

When the data doesn't satisfy the Nyquist Theory, the following equation is working:

$$\oint \nabla P(\vec{r})dr = \sum residues = 2\pi * charge \quad (3-12)$$

Depending on the direction of the circle it has, the residue can be +2π or -2π. These points marked by the residues are not good since they don't satisfy the Nyquist theory, so that we need to treat these residue points separately. This operation can calculate the charge number at the center.

In the analysis program, we set the center of the four adjacent points as the position for the residue. In the meantime, the charge is designated as 1 or -1 depending on the calculation. The unwrapping path should never circle such a charge. The charges with opposite signs are connected, which is called balanced. The lines between the charges are not allowed cross when the unwrapping procedure is being done. This algorithm blocks the propagation of the local error efficiently. The way to connect two points in the program is relatively simple. In the program, I use a connection indicator matrix to represent the branch cut with 1 for branch-cut region and 0 for good region. I take the slope of two points which are supposed to be connected, and then I use the integer length, slope and the round function to get the index of the branch-cut points.The illustration is shown below:

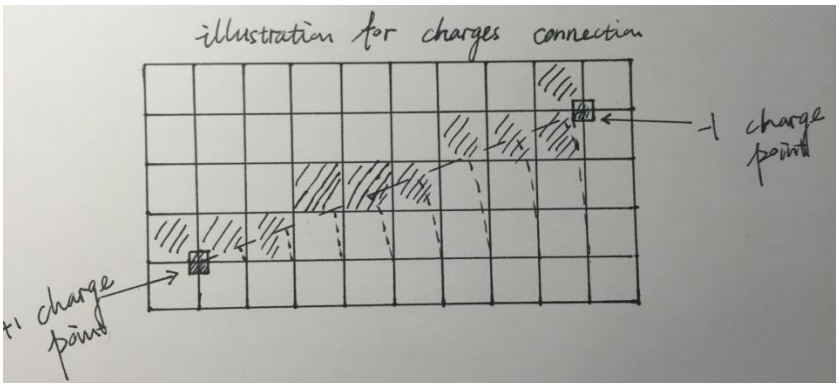

Fig[3.11].Points connection

The building branch cut method is use the integer length from 1 to the maximum integer within the distance between two charge points. Then use the length times the sine and cosine of the angle between the connection line and the x axis. Then use the round function which is supplied by Matlab to find the index of the adjacent cell. Finally, mark the entire line cell in the indicator matrix. In the program, we used 1 to represent the branch cut and 0 represent the valid cell.

The next problem is how to find the optimized charge pairs. There are many ways to do it. We can assign the summation of the length for all the pairs to be a function L:

$$L(x_i, y_i, l_j, m_j) = \sum_{i,j} \left[(x_i - l_j)^2 + (y_i - m_j)^2 \right] \qquad (3-13)$$

Where (x_i, y_i) represents the i^{th} point in the positive(negative) points. The (l_j, m_j) represents the j^{th} point in the negative(positive) points. By reaching the L function's minimum point, we can get the best strategy for the pair choosing. The algorithm to do this optimize is evolutionary algorithm, which is a general and wide applied method. However, when facing too many points, this algorithm is not working that ideally. In this bachelor graduation thesis project, the algorithm with the evolutionary algorithm is not optimized and need more works in it. However, this algorithm is perfectly suitable for this program. If the time is permissible, I would like to write the evolutionary algorithm for the branch cut pair. In this thesis, by referring to a much simple algorithm, the tree search algorithm is proposed.

The algorithm to find the suitable branch cut is introduced subsequently. This tree searching algorithm has the advantage that the speed is really quick. Compared to other algorithm, it can use 1/10 time of other methods since it needs less calculation. However, the drawback of this method is also significantly. It can only find the optimized result when the size of the data is small. In other words, it can't connect the charge point with the other which is far from active one. This drawback can make a high deviation from the optimized result. In the other perspective, it actually provides us with the method to figure out the problem and is with a good convergence.

For the searching, I take advantage of the method from the tree searching. First, marked all the charge points with 1,0 and -1. Then use the left upper elements of the charge as the current points. Next, find all the 8 neighbors of the active charge point to check if there are points at the edge of the graph, if so, connected these two and continue searching for the next charge. When the charge is not adjacent to the edge, we will try to find the unbalanced charge around the active one. If the charge is different with the active charge, connect these two and set the charge as balanced. If the charge or the neighbor is not the same, make the neighbor charge as the active charge and do the iteration. In the same time, this branch should be marked with double the charge. The iteration will continue until the charge is balanced. Then, continue doing this until all of the charges are connected and balanced. Finally, we will get a branch cut map which indicates where the bad region is.

Then use the unwrapping function to unwrap the rest of the phase map. At the end of the unwrapping, do the unwrap process to the branch cut region with reference of the adjacent unwrapped elements. The algorithm is referred to the floodfill function in windows. In the simplest graph software offered by windows, there is a tool named paint kettle. This tool is help to full fill an area bounded by the line. The same is in our case, we need to process an area bounded by the branch cut. The floodfill algorithm is started from a set point. Then check the neighbors if there is any qualified point of active point. Qualified here means it's not at the

branch cut line and is not the edge of the image. If they are qualified, then do the unwrap process to this neighbor point with respect to the active point. After this, set the processed point as the active point and iterate. When there is no point can be found, the unwrapping procedure is finished. The sample of unwrapping result is shown below:

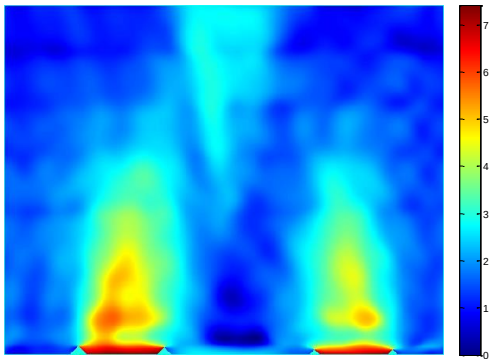

Fig[3.12].Front view of unwrapping

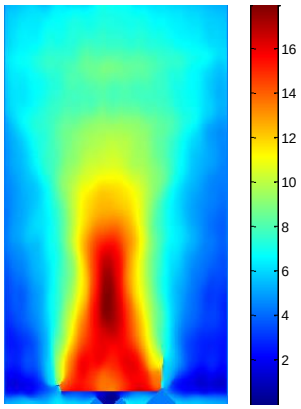

Fig[3.13].Side view of unwrapping

In these two processed samples, we can see the unwrapping algorithm is working fine. The bottom part is the nozzle part. We can already see the outline of the gas density distribution. In the front view image, there are two little bumps at the corner of the rectangular nozzle. This can be discussed latter at the discussion and conclusion part.

3.4 SIRT Tomography

Tomography is the main topic of this thesis. In general, there are two main algorithms of the tomography. One is named as the *Analytical Tomography*, another is named as *Iteration Reconstruction Tomography.* The analytical tomography has the advantage that it has a high speed and accurate theoretical result. However, it needs exact complete information for the boundary. Not only the phase but also the accurate shape of the nozzle needs to be input as known value to the formula to get the result. This is very hard to realize in experiment. In comparison, the iteration tomography needs less information. It needs iteration time to find the fittest solution to current data. In general, analytical tomography

method can get the 3D result, for example the resolution is 960*1280, in less than 1 minute. For the iteration method, it needs more than a day. However, iteration method is much preferred since the set of the boundary information is nearly impossible to get experimentally.

This thesis used an advanced method of iteration reconstruction. Simultaneous Iterative Reconstruction Tomography inherits the property of the iteration method. It can generate a profile perfectly fit the data and has a good convergence. The idea of this method is taking the average. The difficulty for this method is mathematically calculating the area of the cell passed by the beam in different angles. In this project, the mathematical problem is not shown up since only two angle data appear, which is absolutely good and easier. Theoretically, the more angles are, the more accurate the tomography is. That's the reason why in medical treatment, patient should take X ray CT to help doctor to diagnose their symptoms.

As the thesis discussed above, for the asymmetric gas profile, we can't use the Abel Inversion to get the result. Thus the Simultaneous Iterative Reconstruction Tomography method is in the position to do the job. This algorithm is exactly with the idea of ART method. We take the average of the data we got to refine the gas profile. In the data, we have absolute phase shift information. So the relationship between the density and the phase shift should be investigated.

The absolute phase shift P has the relationship with the refraction index of the gas that:

$$P = \frac{2\pi}{\lambda}\int_0^L [n(x) - 1]dx \qquad (3-14)$$

Where the integration is along the axis of laser propagation. λ is the wavelength of the laser. L is the length of the laser path inside the target. n is the refraction index of the gas at position x. In the program, the summation form is preferred:

$$P = \frac{2\pi L}{\lambda}\sum \frac{(n_i - 1)}{s} \qquad (3-15)$$

Where L is the length of the beam path inside the gas target. n_i is the refraction

index of the i^{th} cell in the path. S is the number of cells in the path. The phase shift can be calculated through this method.

As I have shown before, the phase shift maps which are got from experiments contain the information for different heights. In the reconstruction, the SIRT method requires to cut the phase shift pattern into the 1D array, which means the reconstruction should be done layer by layer.

From the graph, the resolution of the reconstruction gas is the same with the CCD camera we used in experiment. The size of the reconstruction result is a rectangular box, which is treated as a N*M matrix in the program. N is equal to the column number of side view data and M is equal to the column number of front view data. The SIRT iteration formula is shown as follow[21]:

$$f_{ij}^{k+1} = f_{ij}^{k} + \alpha \left[\sum_{nm} \left(w_{ijmn} * \frac{\varphi_{mn} - \sum_{ij} w_{ijmn} f_{ij}^{(k)}}{\sum_{ij} w_{ijmn}} \right) \right] * \left(\sum_{nm} w_{ijmn} \right)^{-1} \quad (3-15)$$

Where i,j is the index for the gas target with a specific height. K is the iteration index. α is the sensitivity parameter, which is range from 0 to 2. N and m is the index of the beams with different perspectives. W is the area of the nm beam for the index ij cell. The illustration graph is shown as follow:

However, in our case, we only have 2 angle data. The equation should be:

$$f_{ij}^{k+1} = f_{ij}^{k} + \frac{1}{2}\alpha \left[\left(\varphi_{frontj} - \sum_{i} f_{ij}^{(k)} \right) * \left(\sum i \right)^{-1} + \left(\varphi_{sidei} - \sum_{j} f_{ij}^{(k)} \right) * \left(\sum j \right)^{-1} \right] \quad (3-16)$$

Assume that the data we got from experiment is orthonormal to each other, in other words, the data is taken from two perpendicular perspectives. Different from that of the general algorithm, the area of the reconstruct cell is the same in our project. We can set the error as:

$$error = \frac{\sum_{ij}\left(\varphi_{frontj} - \sum_i f_{ij}^{(k)} + \varphi_{sidei} - \sum_j f_{ij}^{(k)}\right)}{\sum_{ij}\left(\varphi_{frontj} - \sum_i f_{ij}^{(k-1)} + \varphi_{sidei} - \sum_j f_{ij}^{(k-1)}\right)} \qquad (3-17)$$

Theoretically, the error should approach to 1 when the iteration index k approach to infinite, that is:

$$\lim_{k\to\infty} error(k) = 1 \qquad (3-18)$$

We can set that the iteration will be killed when the difference between the error and 1 is less than 1%. Under the test of the program, we figure out the algorithm need roughly 150 iterations to obtain the desired result. We can reduce the iterations by increase the sensitivity parameter. However, in the test, we found that the algorithm has a good convergence performance when α is around 1. In the real data processing, 1 is designated to α.

The reconstructed f is shown as follow:

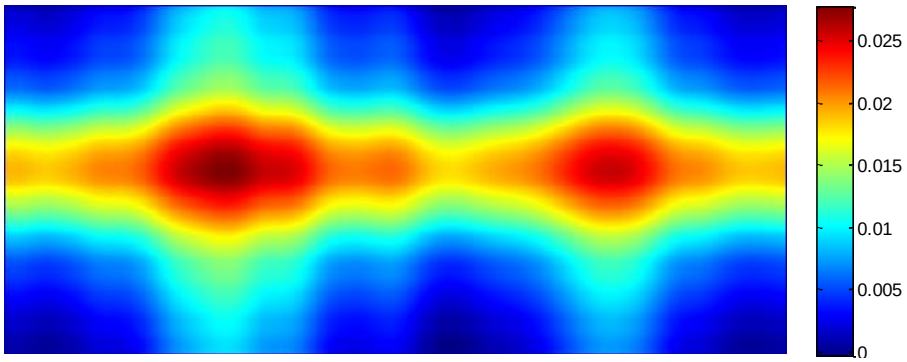

Fig[3.14]reconstruction result for f_{ij}

This is not the end of the project. f_{ij}, in the calculation, should have the dimension with rad/m. After this procedure, the phase shift for the gas target is complete. However, the density of the target should be calculate with the equation:

$$n_{ij} = \frac{f_{ij}\lambda}{2\pi} + n_0 \qquad (3-19)$$

Where n_0 is the refraction index for the background matter. In our case, since the experiment is in the vacuum chamber. We can simply assign 1 to n_0. The relationship between the density and the refraction index is shown below:

$$d_{ij} = \frac{2}{3}\left(\frac{n_{ij}-1}{A}\right) \qquad (3-20)$$

Where A is molar refractivity of the gas.

Molar refractivity[23], A, is an essential internal parameter to show the total polarizability of specific matter. The substance is with unit molar in general. This index is dependent on the pressure, temperature and the refractivity we got in the calculation above. The definition of the molar refractivity is:

$$A = \frac{4\pi}{3} N_A \alpha \qquad (3-21)$$

Where α is the mean polarizability of a simple molecule. N_A is the Avogadro Constant. For a gas, the molar refractivity can be approximated by:

$$A = \frac{RT}{p} \frac{n^2 - 1}{3} \qquad (3-22)$$

The molar refractivity has the dimension with $^{m^3}/_{mol}$. After substituting the molar refractivity into the relationship between density and refraction index, the dimension should be $^{mod}/_{m^3}$. By simply dimension translation we can get the result with the dimension $^{n}/_{cm^3}$.

The procedure is quite clear and simple. But, in the calculation equation of A, we see that the pressure is needed. In the experiment, we only know the pressure inside the pressure, or at the adjacent area of the opening gate. We need the pressure in the gas at relatively far from the opening. The background for experiment is high quality vacuum. The pressure of the gas varies from 5bar to 50bar. The height of the gas is about 1-2cm. Suppose the pressure distribution is linear, which is totally wrong of course, just for getting the feeling of the pressure gradient:

$$\nabla P = \frac{50bar * 10^6 Pa/bar}{1cm * 10^{-2}\, ^{m}/_{cm}} = 5 * 10^9\, ^{Pa}/_{m} \qquad (3-23)$$

The pressure gradient is too high. In this regime, we called the gas jet is supersonic. At high flow velocities, like our case, the Bernoulli's equation used in incompressible flow is not valid. We need a systematic method to find the estimation of the pressure at specific height of the gas target. For the time reason, I don't put so much time on this problem. This problem needs a very critical and

deep systematical knowledge about the supersonic flow. It can be learned in details with the book named "Modern Compressible Flow".

An accurate and sophisticate measurement for the static –pressure rise along different axis of the nozzle just downstream between the throats of the nozzle is done in Caltech's Jet Propulsion Laboratory. To qualitatively study the pressure of the supersonic gas, the graph is enough for the estimation of the gas[24]:

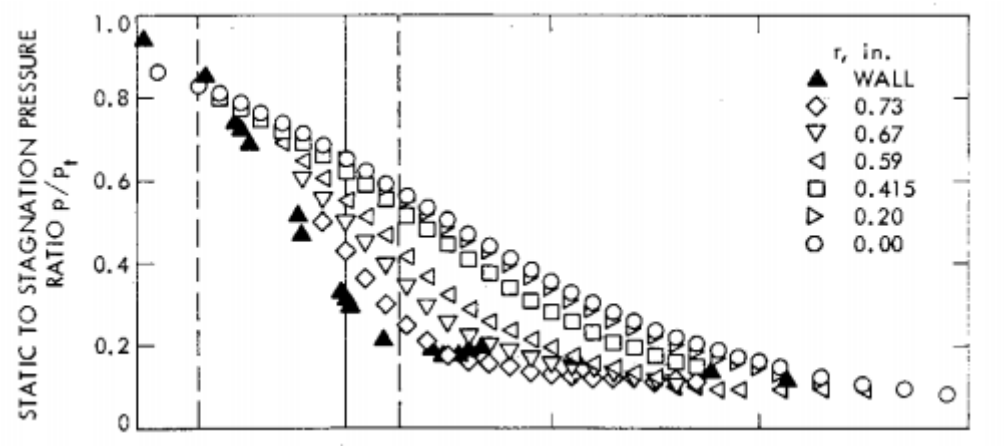

Fig[3.15].Pressure ratio for the position before and after the throat of nozzle

In the figure above, we can see the gradient of the pressure is relatively enormous. We can use the quasi-one dimensional flow theory to estimate the density of the gas. For estimation, the one dimensional compressible gas model should be learned.

What's the definition of the one dimensional compressible gas? Actually, the one dimensional flow should have all its properties changing in one coordinate direction. In other words, the temperature T, density ρ, velocity v and all the other unmentioned properties are the functions of x only, where x is the position coordinate. This is the simplest model since it can be solved with analytical solutions. In fact, the project we are facing should be applied with the 3D compressible flow model. However, we don't have enough time to do the numerical simulation. 1D model should be relatively acceptable here.

The same as the case we have, the area of the nozzle is changed with distance x. The cross section of the slit supersonic nozzle is shown below:

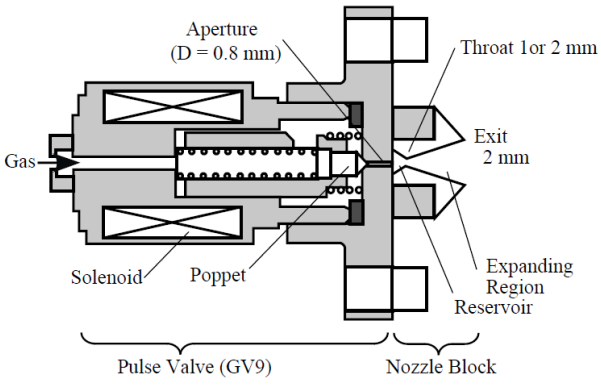

The cross sectional view of our nozzle.

Fig[3.16].Cross section of the slit nozzle

The equations for the one dimensional flow can be obtained by the conservation law which is ubiquitous in hydrodynamics[25]:

$$-\oiint \rho\vec{v} * d\vec{S} = \frac{\partial}{\partial t}\iiint \rho dV \qquad (3-24)$$

Where $\vec{v}$ is the velocity of the stream. ρ is the density of the flow. $d\vec{S}$ is the area element. dV is the volume element. If the flow is a steady flow, which means the density distribution doesn't change with time t. This relationship can be:

$$\rho_1 u_1 A_1 = \rho_2 u_2 A_2 \qquad (3-25)$$

Where 1 and 2 is for the different positions. Similarly, for the momentum conservation, we have:

$$\oiint (\rho\vec{v} * d\vec{S})\vec{v} + \iiint \frac{\partial(\rho\vec{v})}{\partial t} dV = \iiint \rho\vec{f}\, dV - \oiint p d\vec{S} \qquad (3-26)$$

Where $\vec{f}$ is the force applied to the flow element in the integral volume. P is the pressure at the surface of the volume. This equation is nothing but for the integral volume:

$$\vec{F} = \frac{dp}{dt} \qquad (3-27)$$

Similarly, when the flow is a steady flow, we have:

$$p_1 A_1 + \rho_1 u_1^2 A_1 + \int_{A_1}^{A_2} p\, dA = p_2 A_2 + \rho_2 u_2^2 A_2 \qquad (3-28)$$

And the energy conservation gives:

$$h + \frac{u^2}{2} = const \qquad (3-29)$$

where h is the enthalpy of the gas. u is the velocity of the flow element. By substituting the relation in thermodynamics into the hydrodynamics, we can get the result[25].

Suppose the flow inside the nozzle is an isentropic flow, by the three conservation laws above, we can simply imply that:

$$\frac{p}{p_0} = \left(1 + \frac{\Upsilon - 1}{2} M^2\right)^{\frac{-\Upsilon}{\Upsilon - 1}} \qquad (3-30)$$

$$\left(\frac{A}{A^*}\right)^2 = \frac{1}{M^2}\left[\frac{2}{\Upsilon + 1}\left(1 + \frac{\Upsilon - 1}{2} M^2\right)\right]^{\Upsilon+1/\Upsilon-1} \qquad (3-31)$$

Where p is the pressure we need. Υ is the quotient of specific heat for the fixed pressure and fixed volume. M is the Mach number of the gas. A is the area in the gas nozzle in different position. In the experiment, the Mach number is 5.

Since the Nitrogen is double atom molecular, we theoretical believe Υ should be 7/5. After simple calculation, the result is:

$$\frac{p}{p_0} = \left(1 + \frac{\Upsilon - 1}{2} M^2\right)^{\frac{-\Upsilon}{\Upsilon - 1}} = 0.0019 \qquad (3-32)$$

The supersonic gas nozzle has a special throat structure to create high pressure gradient inside the nozzle. In this case, the pressure before the throat should be the number we read out from the experiment. After the throat, assume our nozzle has the supersonic velocity 5 mach. The pressure outside the nozzle should be around 0.002 of that of the inside the throat, which is around:

$$p = 30 * 10^4 * 2 * 10^{-3} = 600\text{mbar} \qquad (3-33)$$

This pressure is very near the pressure of the atmosphere. During the experiment, we can clearly see the changing in the pressure. It needs roughly 30s for the vacuum pump to regain the aim pressure. We see from the equation that the pressure out the throat doesn't change that much with the distance x. However, in the free expanding model, we know the pressure decrease exponentially. This also applies to the case we faced here. The outside pressure located at the tail of the

exponential function. The similar result should be regained.

Having identified the pressure, we can calculate the molar refractivity. The coefficient is multiplied to the reconstruction result. Here we used the data with 30bar to reconstruct the density. The result with the dimension $^{n}/_{cm^3}$ is:

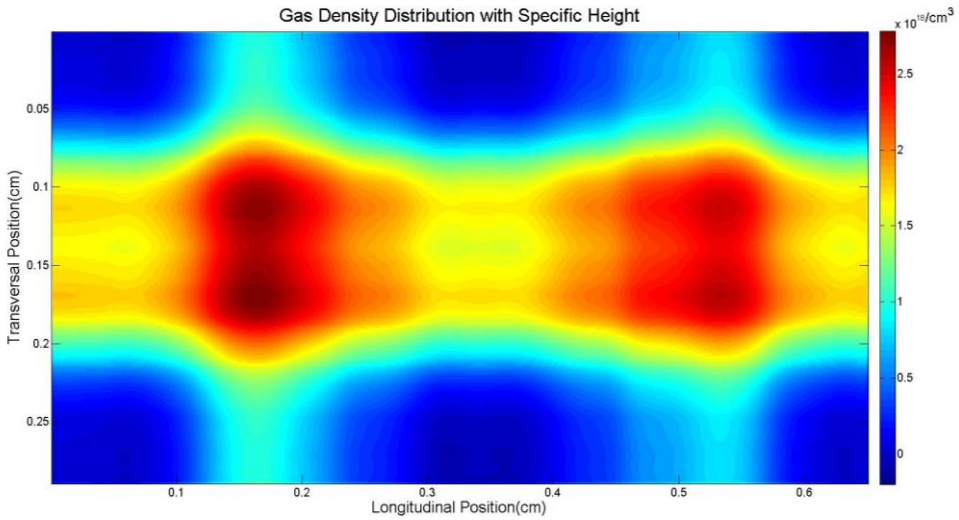

Fig[3.17].reconstruction for height 0.5mm

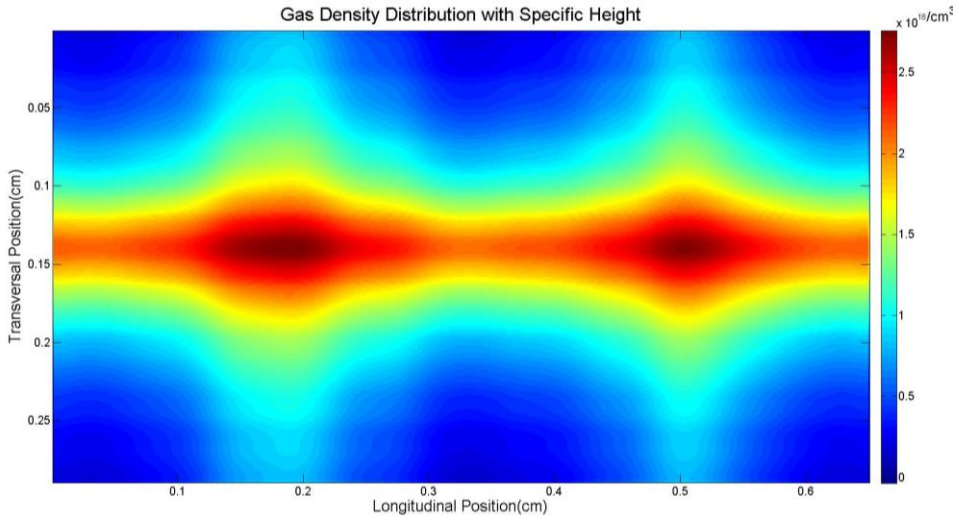

Fig[3.18].reconstruction for height 1mm

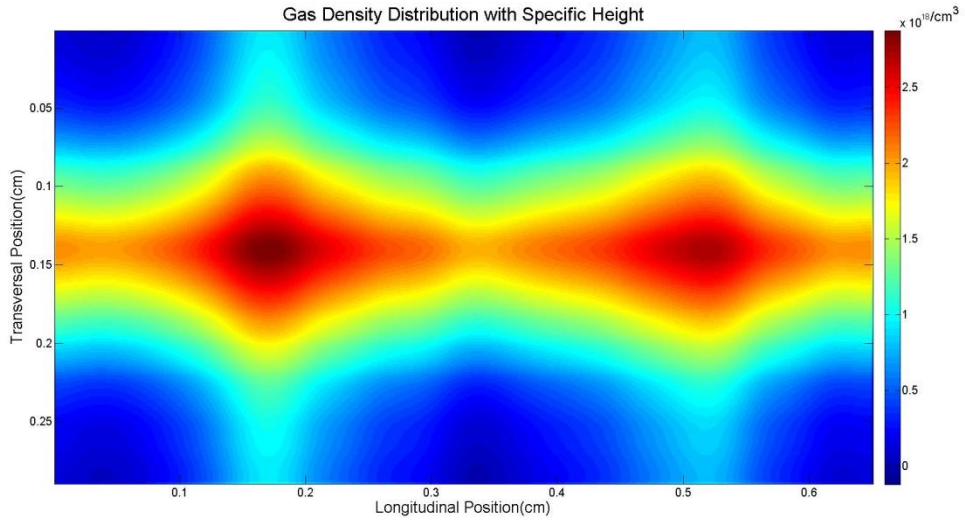

Fig[3.19].reconstruction for height 1.5mm

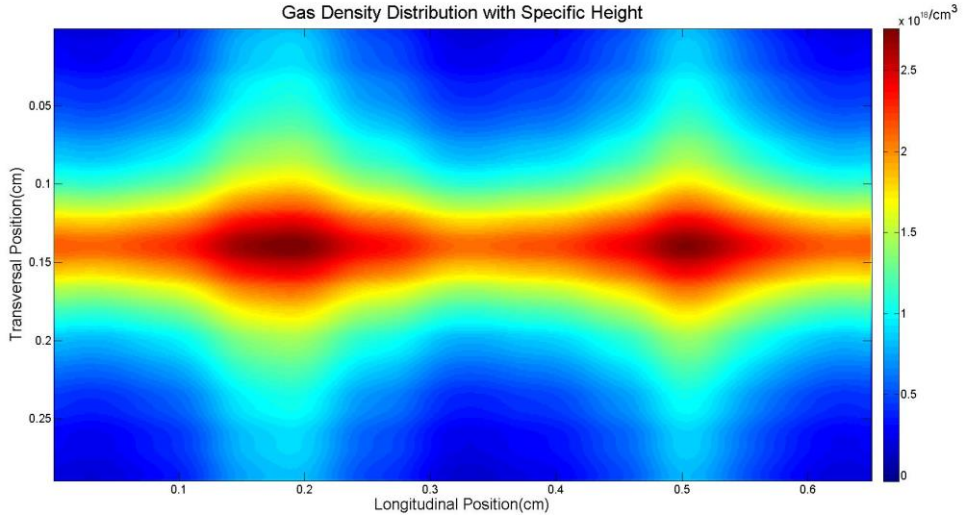

Fig[3.20].reconstruction for height 2mm

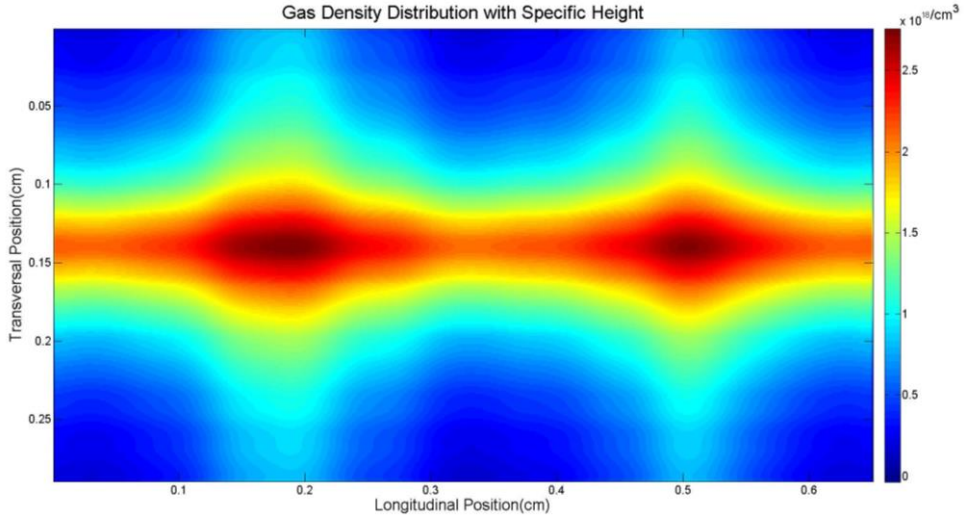

Fig[3.21].reconstruction for height 2.5mm

In all of the graphs above, the x-axis represents the longitudinal position of the

gas distribution and y-axis represents the transversal position. The dimension for the position is centimeter. The order of the density is higher than $10^{18}/_{cm^3}$.

From the result provided by the group in University of Tokyo, the result should be in the correct order. In their research, the density has a relation with the pressure that:

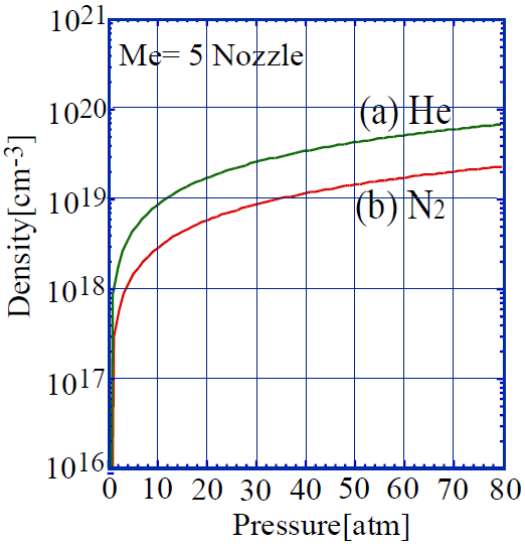

Fig[3.22].Density verses Pressure[26]

However, it also depends on the profile and area of the orifice. We actually see the same order or density in the experiment we did. Moreover, in our case, we plot the longitudinal density profiles for the rectangular nozzle at different heights. The axis is at the center of the nozzle. For the size of the nozzle, the width is 1mm and the length is 4mm. The longitudinal density distribution for 25bar is shown below:

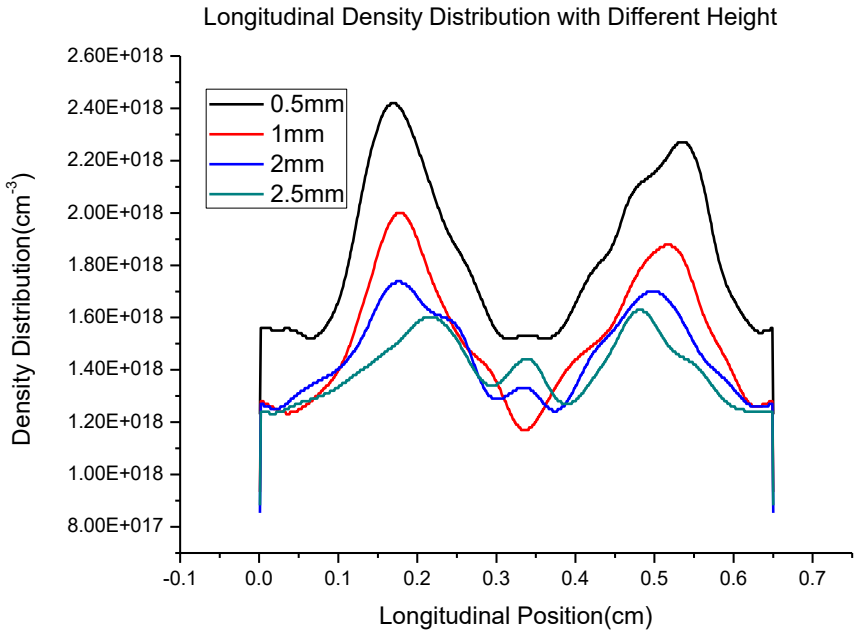

Fig[3.23].longitudinal density distribution of the rectangular nozzle at different heights above the nozzles opening gate(Edge)

In the graph above, the different color line represent the pressure for different height. The x-axis is for the position in longitudinal direction. Y axis is the density. We see that as the height getting bigger, the density is smaller. This is pretty reasonable. The density of the gas should reach its maximum at the base of the nozzle. After that, the supersonic gas coming from the nozzle does a free expansion to the vacuum chamber. As the expansion going, the density of the gas tends to reach a local quasi-equilibrium at a high position. On the other hand, the difference of peak density and valley density tend to get smaller. See the black line which represents the height with around 3mm, the relative difference is much smaller than that of the yellow line which represents around 0.6mm from the nozzle orifice.

An interesting phenomenon happens when we check the gas density distribution for the nozzle's longitudinal center axis. The axis chosen here is the center of the slit nozzle. We can get the density profile is:

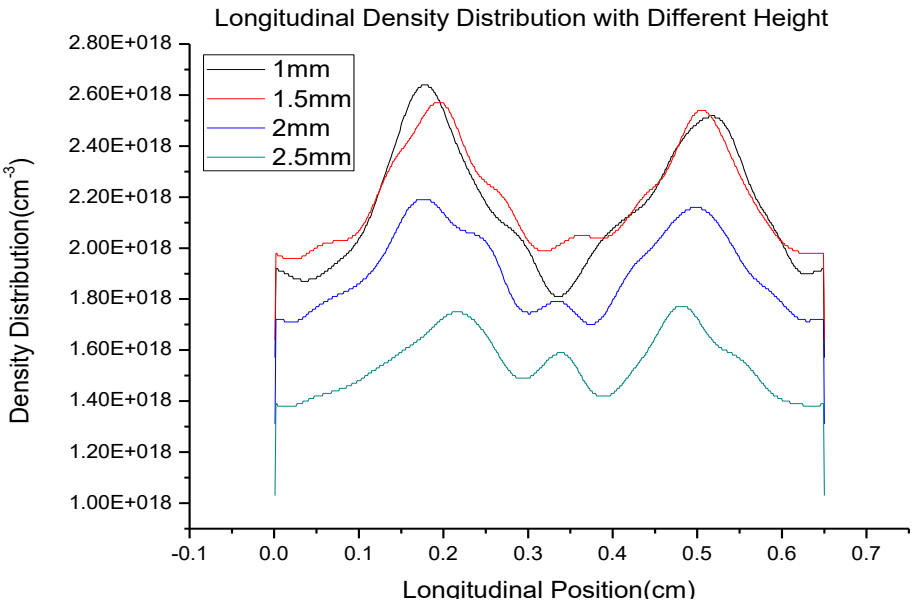

Fig[3.24].longitudinal density distribution of the rectangular nozzle at different heights above the nozzles opening gate(Center)

There is a mixing area at around 1.5mm from the orifice. The density doesn't change that much for the center. Actually, it seems like the density is very stable at this regime. To check out the phenomenon, we do the same work for the 20bar data.

We did the same work for the transversal density distribution, both for the center axis and the edge axis with pressure 20bar.

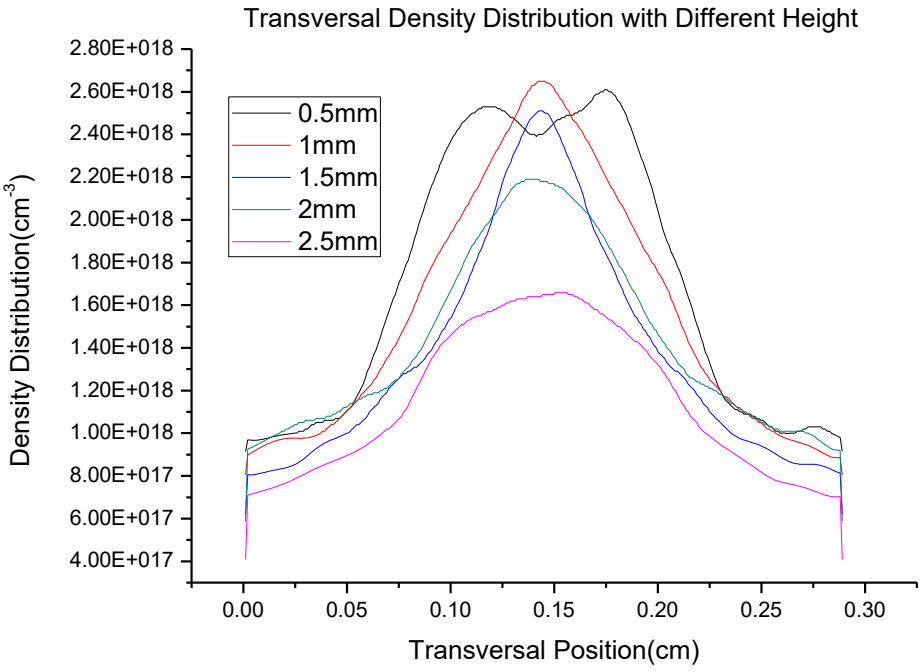

Fig[3.25].Transversal density for the edge

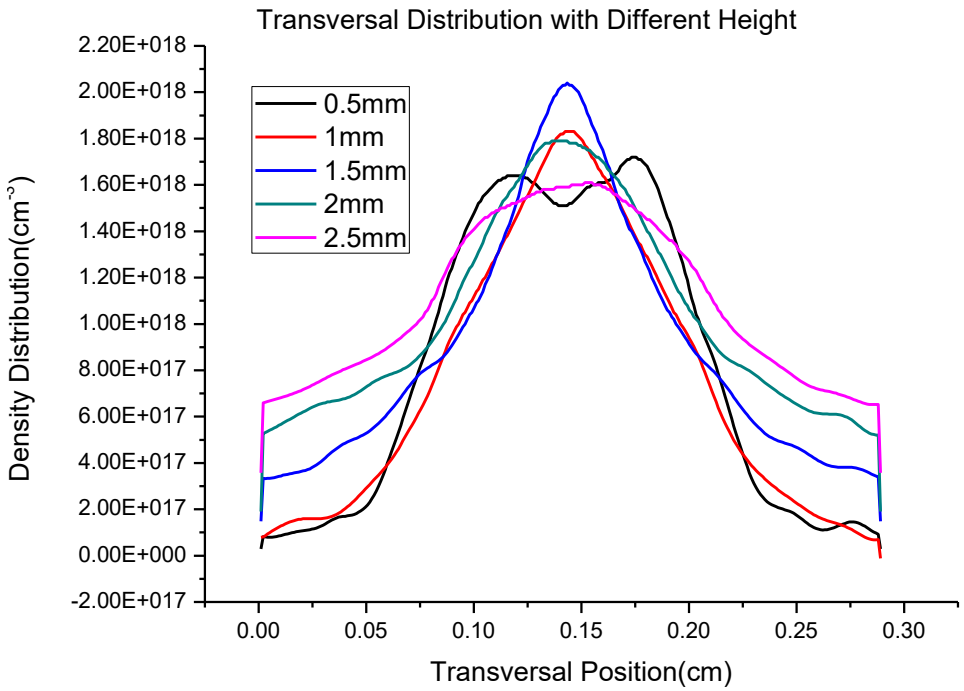

Fig[3.26].Transversal density distribution for the center axis

From these two plots, the transversal density distribution is shown. The profile of the gas is perfectly a peak at the center of the slit nozzle. We can see the difference clearly for different axis. We find that above around 2mm from the orifice. There is a flat density distribution at the center. In this sense, we plot the 2mm height for several different pressure, the result is as follow:

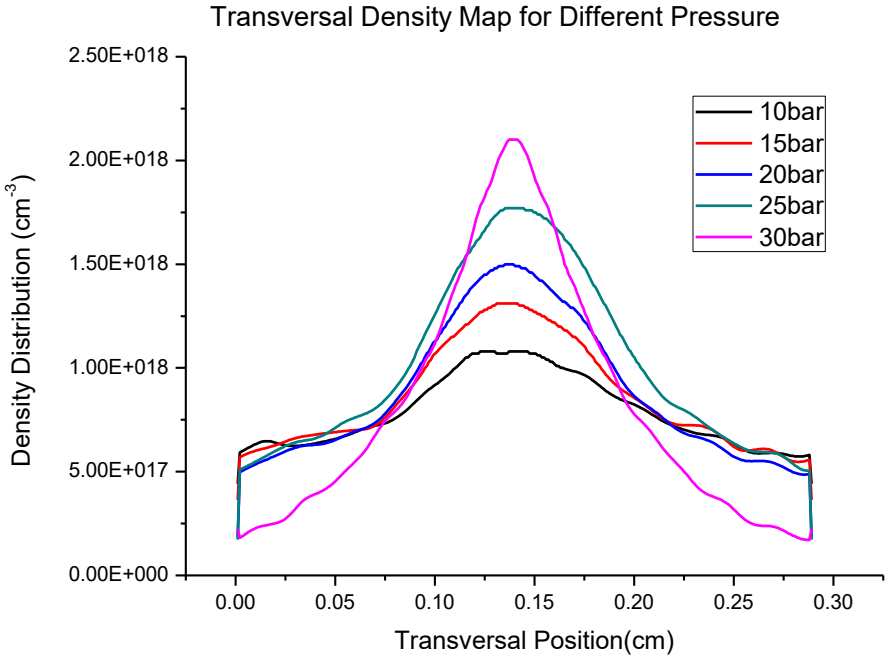

Fig[3.27].Transversal density for the different pressure

We do a Gaussian fitting for the density map. In electron acceleration experiments, we always need to focus the main laser in a spot. However, sometimes we don't know if the position of the focus is qualified or not. Here we use a qualitative result to define the focus spot. After we do the Gaussian fitting with treating the gas as free expansion into vacuum, we calculate the FWHM of the Gaussian. The Gaussian fitting line is shown as follow. Then we define that the focus spot is qualified when it's within the length of 2FWHM around the center, which is:

$$Focus\ spot \in [center - FWHM, center + FWHM] \qquad (3-34)$$

Gaussian Fitting for the Transversal Density Distribution

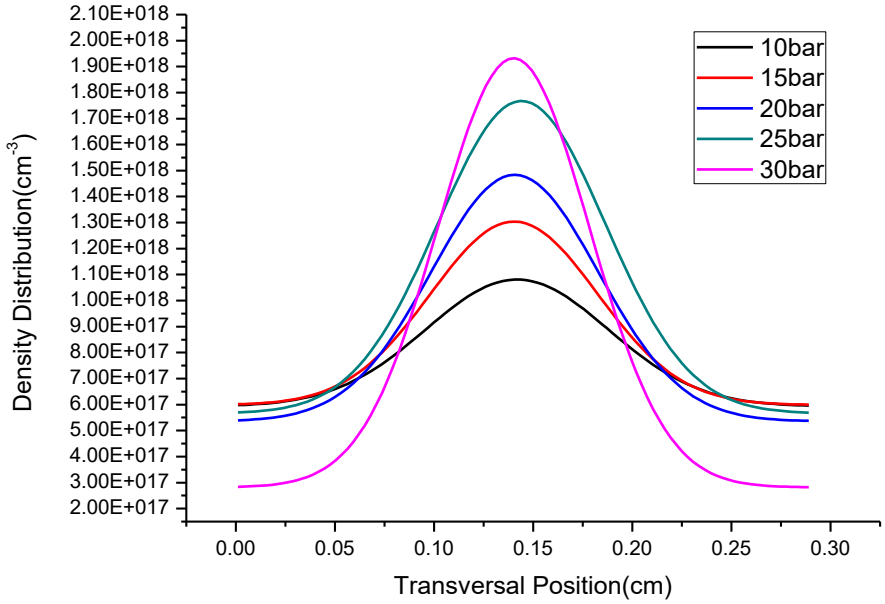

The result for linear fitting of FWHM is as follow:

Linear Fitting for Density FWHM

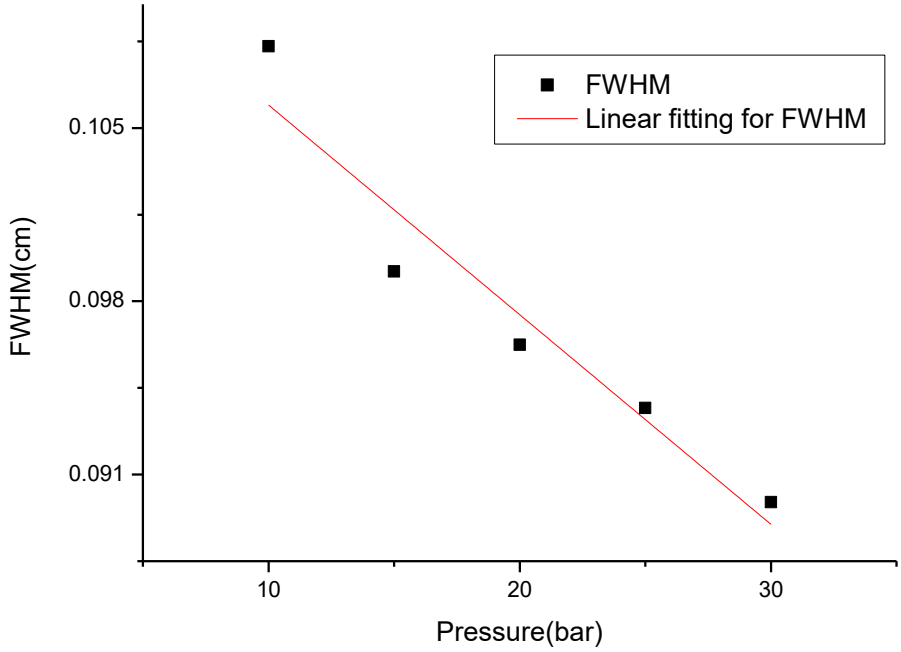

Fig[3.28].Linear fitting for the qualified range for laser spot

The x-axis represents pressure with dimension bar. The y-axis represents the FWHM with dimension cm. We can see from the graph, the FWHM doesn't change very much with the pressure increasing. When doing experiment, we need to focus the beam at around 2.5mm and the focus spot should be focused within 1mm at the center of the orifice. More, the flat area increases with the decreasing of the pressure. However, we can notice that the density of the gas is obviously increasing with the pressure at the same height. In the experiment, if we want to get a high density gas target, we need to increase the pressure and levitate the focus spot. Raising the focus spot is because we assume that we always do the experiment in high density part of the gas target. When we are doing the experiment far from the orifice, the gas target could be a dilute underdensed one. The experiment usually is not performed at that regime.

In order to show the density variation more clearly, the curve graph below picks the center of the orifice as the reference point. The density is plotted as the function of height. The x-axis is for the distance with dimension centimeter. The y-axis is for the density at the reference point. From the graph, we find that the density reaches its maximum point at nearly 1.5mm far from the orifice. However,

as the pressure increasing, there is a tendency that the maximum density height is delayed. After the maximum point, the density of the gas will decrease monotonically.

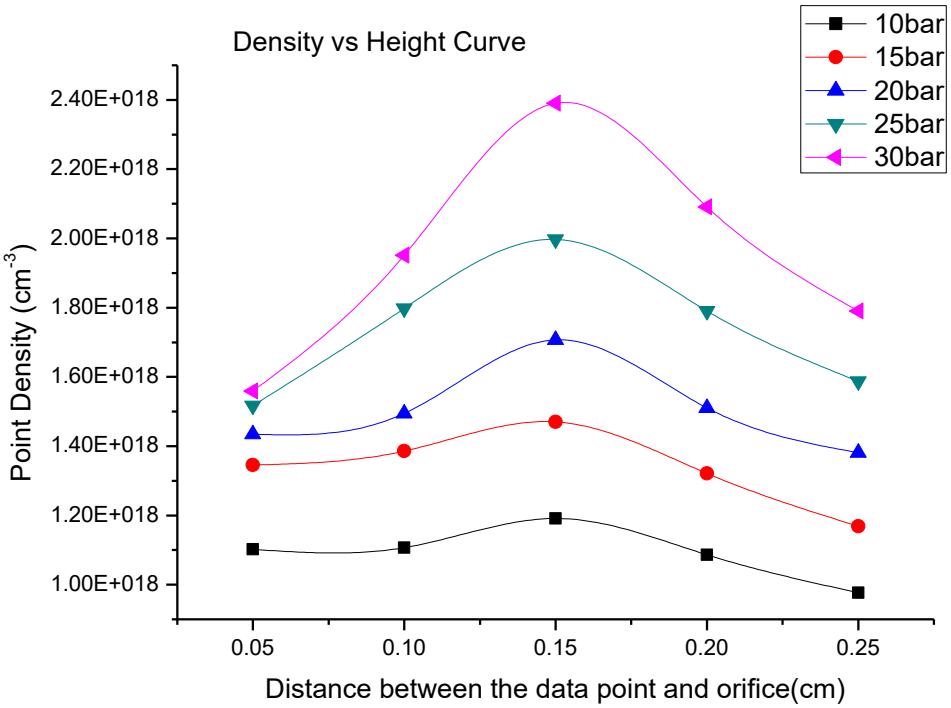

Fig[3.29].Density plot as a function of height for different pressure gas

The reason why the density peak isn't at the base needs more sophisticated explanation. I think it has some relations with the trigger delay of the camera. The CCD camera takes the image of the inference pattern after the nozzle is close. The main part of the nozzle is expanded into the vacuum. Actually, we can already see this phenomenon in the row data. Following is a sample side view interference pattern taken from 25bar experiment.

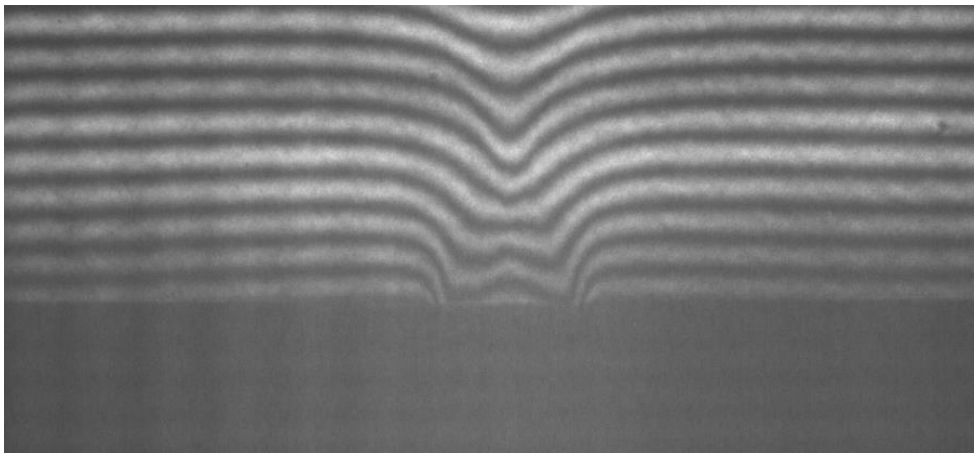

Fig[3.30].Side view pattern for 25bar experiment

The width of the orifice is 1mm. The fringe should tilt down if the media refraction index is larger than that of the vacuum. However, in the middle part of the pattern, we see the fringes tilt up. This shows that the density at the center is lower than the surrounding media. However, in this case, the density reaches the peak at around 1.5mm height. The same things happen in my colleague Haohan's work. He also gets the density reaching the maximum at the middle way in the vacuum. To find the explanation, we need to do the simulation with the compressible fluid. That's another topic which I want to study.

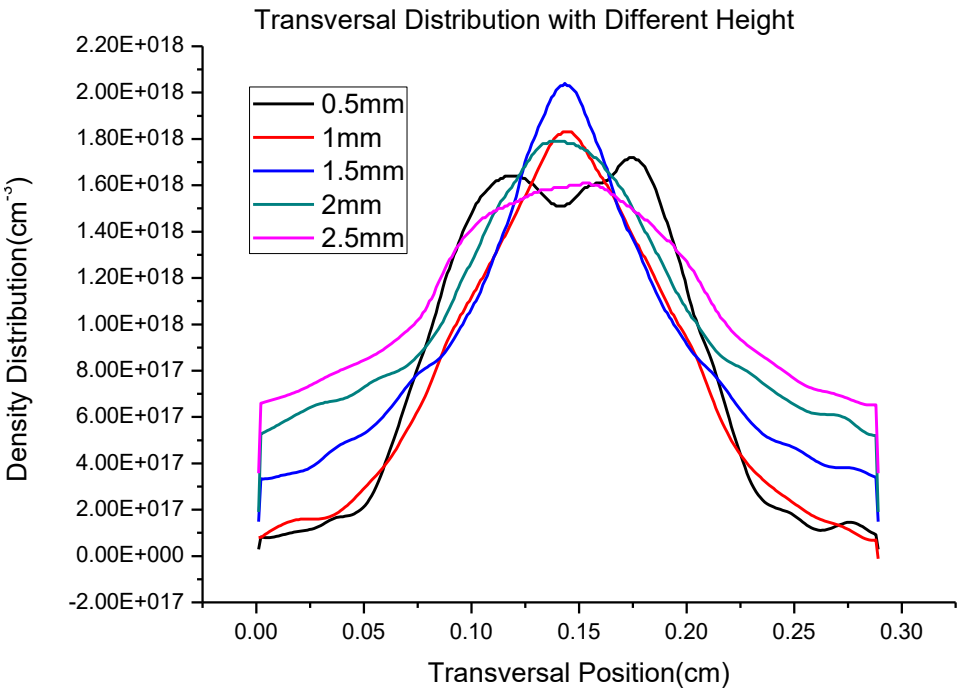

Fig[3.31].Transversal Distribution with Different Heights

As we can see in the plot above, as the height turns up, the gas target trend to expand and have a lower density than the bases. Near the base of the nozzle, the density is much higher at the width edge of the nozzle. For the usual nozzle, this phenomenon happens. However, for the supersonic nozzle, the density distribution is not the same. Theoretically, the density should be like a diamond. That's the reason why the h150 and h200 are always tangled together. The difference between these two heights is very small. Instead of saying that the difference is small, we prefer to explain that the turbulence of the gas target is

shown up at near 1-2mm far from the nozzle. By considering the mechanism of LWFA, the density is a quite stable region. Maybe this region can find some interesting phenomena in the electron acceleration experiment.

In addition, after processing the whole phase image, we find that the density have a quasi-periodical appearance. That's to say, the density has a very blurry periodical peaks and valleys in around 2cm. The gas density 1cm far from the orifice is not high enough to generate qualified plasma. Thus, we only care about the adjacent are of the nozzle's slit, because the density is suitable for the electron experiment. In the data process, the rest of the graph is cut.

Moreover, the wall of the nozzle makes the gas much likely "attached" to the edge. We can clearly see that the density at the edge is larger than that of the center. When the position get higher, the density difference between the near wall and the center is diminished. This is caused by the diffusion of the gas. More, the density plots versing the different pressures from 5bar to 30bar at the 2mm height are also plotted below:

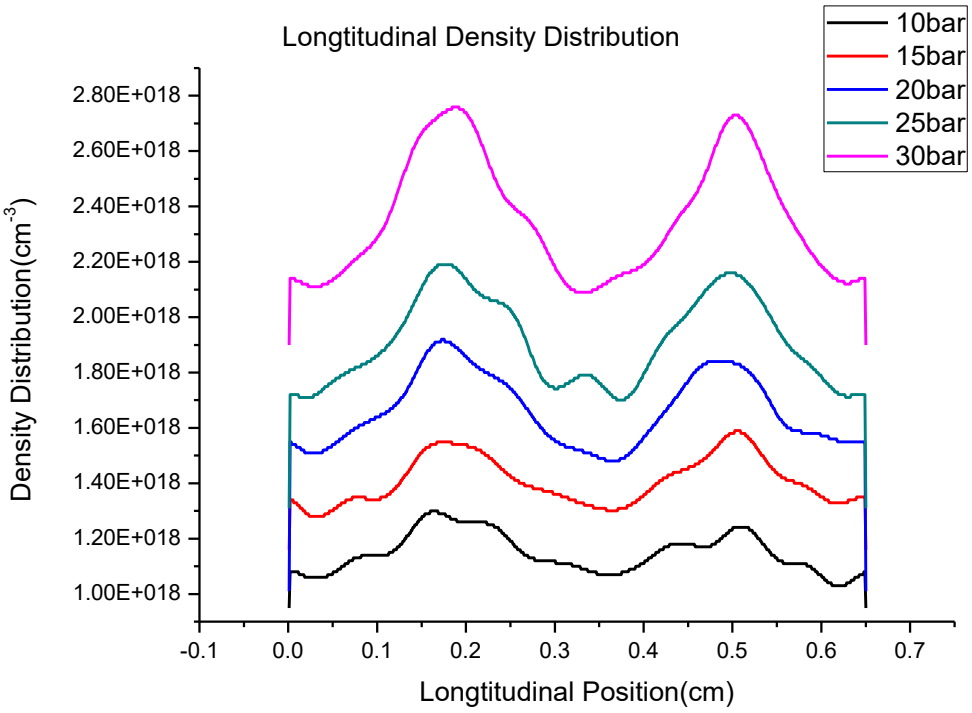

Fig[3.32].Longitudinal density distribution of the rectangular nozzle for different pressures

It's obvious that there is a valley at the center of the orifice. This is a very

interesting profile for the LWFA experiment. It will be discussed in detail in the following part.

From the plot, we also see a clear correlation between the pressure and the density of the gas target at a high position. However, the relationship is not linear. Close to the opening, the change is quite small. The linear fitting of the density at the center of the orifice is shown below. We pick two different heights. 0.5mm and 2mm is chosen:

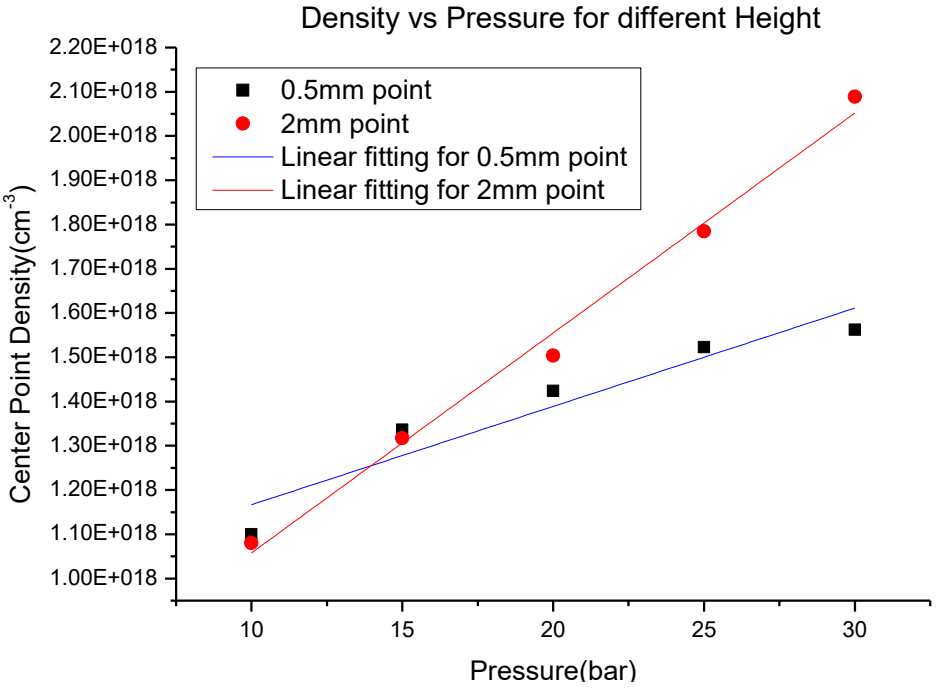

Fig[3.33].Density of the center point of rectangular nozzle for different pressures

In this graph, we see that the linear relationship between density and pressure is quite different for the 0.5mm point and the 2mm point. For these two points, we find that:

$$R\_square_{0.5} = 0.88165 \qquad (3-33)$$

$$R\_square_{2} = 0.98946$$

The correlation between the pressure and density is much stronger for the higher point. However, for the supersonic gas, the explanation should be different from the idea gas. The interaction between particles should be enormous compared to the dilute gas. However, this phenomenon was also observed by the other group in Department of Physics and Astronomy, University of Nebraska, Lincoln.

4 Discussion

The specific arranged experiment gives out the data we need to do the analysis. The analyzing program process these row data and turn them into the fact we want. Till now, the project for the bachelor thesis is finished. However, there are still many works to do to improve the result accuracy.

From experiment, the fringes we get are only span half of the image. We didn't use the entire chip in CCD for the experiment. For the next experiment, we need to adjust the beam size, especially the collimator of the laser, to have a larger beam size. The larger the beam size, the bigger the view we can get. We also need to change the mirror and lens with much bigger one. Not like that of the ultra-short high intensity laser, the imaging system always needs a large valid area to diagnose the experiment instrument. In addition, the beam cutting can highly influence the result. In future, the imaging system should be improved.

Still in the experiment, the distance between the biprism and the force spot can be changed to get a better interference pattern. In the filter part, we see that the filter is based on the frequency. In other words, the density of the fringe should be a little bit higher than that is now. However, we need a graph with clear fringes. In summary, in the full view, 30-40 fringes are sufficient to get a high quality phase map. If the number of fringes is too small, the final phase map will fall for the Nyquist Sampling Theory. If the number of fringes is too big, the phase difference can't be calculated. In the future, a pre-experiment should be done to find the fittest fringe number, which can give out the smallest charge number. When the charge number is not changed, the number of fringes is the less the better.

For the analysis part, as this thesis showed above, filter, unwrapping and tomography are the three main parts for the analyzing system. The box size of the filter is chosen from our own eye. If the time is sufficient, I want to study the relationship between the resolution of the filtered result and the box size. How to get the optimized size of

box is what I want to study deeper. For the unwrapping, the tree searching method for connecting the charges are good, but not the optimized. I want to use the evolutionary algorithm to optimize the charge pairs. That could be a totally different program compared with what we have now. For the most important part, the tomography, I want to use multi angle method to find the accurate result. Right now, the two angle method is only working for the rectangular nozzle. We suppose that there is some degree of symmetry for the nozzle. However, in other case, once we have a weird shape nozzle(this can happen in application, not the experiment), the tomography should also work. The way to overcome the difficulties for the calculation of the area difference, it needs a sophisticated mathematical derivation. It's a little bit hard. Once this works are done, I want to write a program which is qualified for the commercial standard. It should have a clear user interface and background calculation. After this, the total characterization system is finished.

At the end of the tomography, a new problem we never thought before happened. The pressure of the gas needs to be calculated. The supersonic gas, in other words, the compressible gas, has different property with the fluid or incompressible gas. The special property results a strong turbulence at 1mm-2mm away from the orifice. Further simulation about the supersonic gas expansion can explain the phenomenon much better. In addition, we can have a density valley at the near orifice region. We hope to make a wider nozzle opening to do the electron acceleration experiment. This experiment theoretically can reduce the deviation of the momentum spectrum of the accelerated electron.

Moreover, the structure of the supersonic nozzle should be considered further. We still have many problems facing the supersonic gas. In the future, we would like to learn the mechanism of the compressible flow and do an experiment for different Mach number nozzle. After learning the compressible flow dynamics, we'll have the ability to design our own nozzle with specific Mach number for the electron acceleration experiment. Moreover, we can study the phenomenon when two supersonic gas hit to each other. This part could be really fun. We can even find a much better density distribution which can enhance the LWFA.

This project shows a wonderful result and has the potential to contribute to the experiment we are doing in the lab. In summary, the following works should be done to understand the result better. Here is the summary for this part.

Summary of the discussion

What we should do to further improve this project:

1) Improve the imaging system in experiment until the fringe can span the whole chip.

2) Optimized the fringe density in experiment until the data satisfies Nyquist Sampling theorem. Empirically, there should be around 30-40 fringes in the whole view size.

3) Optimize the size of the mask box in the image enhancement procedure.

4) Optimize the pair searching algorithm in Branch Cut procedure, though tree searching is the most efficient one.

5) Do the mathematical derivation to get multi-angles Tomography algorithm. This can obviously improve the accuracy of the result.

6) Study the time evolution of the gas density distribution with supersonic nozzle.

7) Understand the supersonic gas property and do the simulation for the compressible gas expansion in 3D.

8) Study the interaction of the compressible gas. Use the peak-valley-peak structure to do the LWFA experiment. Do the PIC simulation for the peak-valley-peak pattern underdensed plasma.

9) Understand the structure of the supersonic nozzle.

All the problems listed here are deserved to study in the future. Hope the further study can make a good result.

5 Conclusion

We have presented a sophisticated study for the gas target profile produced by an asymmetric supersonic gas nozzle. We applied the interferometry from two orthogonal directions. Then we applied the SIRT algorithm to reconstruct the gas profile for different height and pressure of the target. Our project reveals the characteristics of the gas target from the nozzle. This result can be used to any gas relevant research, especially for the industry. Future work plan are also listed as a reference.

Tomographic measurements were carried out to the rectangular nozzles (with 1mm width and 4mm length). We do a sequence of experiment to study the relationship between the gas pressure and the density of the target. The density distribution for different height and the density distribution along a specific axis are also studied.

From the reconstruction result, the profiles of the gas target at different heights are achieved. Moreover, the density distributions for both longitudinal direction and transversal direction are showed above. We noticed that the edge shows attraction to the gas. From this face, we assume that the friction between the wall and gas is less than that with other gas elements. In the longitudinal direction, we showed the density peak-valley-peak sandwich structure.

In addition, we defined the proper focus spot as the adjacent area of the center point of the peak. The FWHM is changed little with the pressure before the nozzle throat. The FWHM is around 1mm for the nozzle we use in experiment.

We find a clear correlation between the density of the center point and the pressure before the nozzle throat. The linearity is higher with the upper point. In comparison, the point near the orifice showed less density correlation with the pressure. More, the density of the gas reaches its maximum point at the height about 1.5mm from the orifice.

In the experiment, we figure out that the density of the target reach the maximum

value after the trigger time around 10ms. We tracked the density of the gas target with center point in the gas target. The graphs are shown in the data analysis part.

6 Reference

[1] Winick H. Synchrotron radiation.[J]. Scientific American, 1987, 257(5):88-99.

[2] Tajima T, Dawson J M. Laser Electron Accelerator[J]. Physical Review Letters, 1979, 43(4):267-270.

[3] Faure J, Glinec Y, Pukhov A, et al. A laser-plasma accelerator producing monoenergetic electron beams.[J]. Nature, 2004, 431(7008):541-4.

[4] Sprangle P, Esarey E, Ting A, et al. Laser wakefield acceleration and relativistic optical guiding[J]. Applied Physics Letters, 1989, 53(22):2146-2148.

[5] Decreau P M E, Etcheto J, Knott K, et al. Multi-experiment determination of plasma density and temperature[J]. Space Science Reviews, 1978, 22(5):633-645.

[6] Lemos N, Lopes N, Dias J M, et al. Design and characterization of supersonic nozzles for wide focus laser-plasma interactions.[J]. Review of Scientific Instruments, 2009, 80(10):103301 - 103301-5.

[7] Schmid K, Veisz L. Supersonic gas jets for laser-plasma experiments[J]. Review of Scientific Instruments, 2012, 83(5):053304-053304-10.

[8] Semushin S, Malka V. High density gas jet nozzle design for laser target production[J]. Review of Scientific Instruments, 2001, 72(7):2961-2965.

[9] Sylla F, Veltcheva M, Kahaly S, et al. Development and characterization of very dense submillimetric gas jets for laser-plasma interaction[J]. Review of Scientific Instruments, 2012, 83(3):033507 - 033507-7.

[10] Auguste T, Bougeard M, Caprin E, et al. Characterization of a high-density large scale pulsed gas jet for laser–gas interaction experiments[J]. Review of Scientific Instruments, 1999, 70(5):2349-2354.

[11] Colton C, Wilt S, Gilbert D, et al. Characterization of neutral density profile in a wide range of pressure of cylindrical pulsed gas jets[J]. Review of Scientific Instruments, 2000, 71(6):2329-2333.

[12] Feeman T G. Algebraic Reconstruction Techniques[M]// The Mathematics of Medical Imaging. Springer New York, 2010:101-114.

[13] Landsberg G. Black Holes at the Large Hadron Collider[J]. Physical Review Letters, 2001, 87(16):161602.

[14] Chen F F. Introduction to plasma physics and controlled fusion. Second edition. Volume 1: Plasma physics[J]. 1984.

[15] Gibbon P. Short Pulse Laser Interactions with Matter[M]. 2005.

[16] Geddes C G R, Toth C, Tilborg J V, et al. High-quality electron beams from a laser wakefield accelerator using plasma-channel guiding[J]. Nature, 2004, 431(7008):538-41.

[17] Trines R, Bingham R, Najmudin Z, et al. Electron trapping and acceleration on a downward density ramp: a two-stage approach[J]. New Journal of Physics, 2010, 12(17):39-87.

[18] Geddes C G, Nakamura K, Plateau G R, et al. Plasma-density-gradient injection of low absolute-momentum-spread electron bunches.[J]. Physical Review Letters, 2008, 100(21):2539-2541.

[19] By User:Stigmatella aurantiaca, CC BY-SA 3.0, https://commons.wikimedia.org/w/index.php?curid=30147881

[20] By Stigmatella aurantiaca - Own work, CC BY-SA 3.0, https://commons.wikimedia.org/w/index.php?curid=25125975

[21] Golovin G, Banerjee S, Zhang J, et al. Tomographic imaging of nonsymmetric multicomponent tailored supersonic flows from structured gas nozzles.[J]. Applied Optics, 2015, 54(11):3491-7.

[22] Goldstein R M, Zebker H A, Werner C L. Satellite radar interferometry - Two-dimensional phase unwrapping[J]. Radio Science, 1988, 23(4):713-720.

[23] Steen W M. Principles of Optics M. Born and E. Wolf, 7th (expanded) edition[J]. 2000, 32(5):385-385.

[24] Back L H, Cuffel R F, Massier P F. Transonic flowfield in a supersonic nozzle with small throat radius of curvature[J]. Aiaa Journal, 1969, 7(7).

[25] Anderson J D, Anderson J D. Modern compressible flow, with historical perspective - 2nd Edition[J]. McGraw-Hill series in aeronautical and aerospace engineering, 1990.

[26] Development of Wave-free Supersonic Gas jet for Laser Plasma Interaction studies. T.Hosokai, M-Uesaka and K.Horioka. Nuclear Engineering Lab, University of Tokyo

7 Acknowledgement

Thanks for Dr.Thomas Sokollik, who provided me with the chance to learn the researcher's work. Thanks for Dr.Nasr Hafz, who helped me a lot for my bachelor thesis project after Dr.Thomas left. Thanks for my colleague, Haohan Xia and Noaman Haq, who discussed with me and inspired me when there are problems in both experiments and programming.

Thanks for my dearest parents, who support me in both physical life and mental life. Thanks for my colleagues and classmates, who shared amazing four years with me.